Molecular Cell

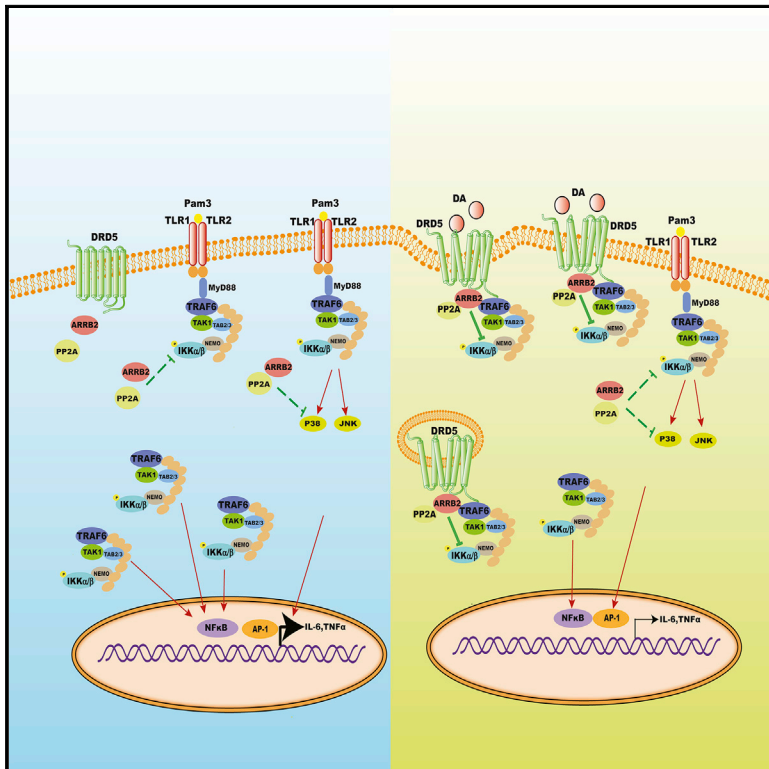# Dopamine Uses the DRD5-ARRB2-PP2A Signaling Axis to Block the TRAF6-Mediated NF-κB Pathway and Suppress Systemic Inflammation

Graphical Abstract

Highlights

- Dopamine inhibits TLR2-induced NF-κB activation and inflammation via the DRD5 receptor

- DRD5 can directly recruit TRAF6 and its negative regulator ARRB2

- DA-DRD5-ARRB2 signaling axis impairs TRAF6-mediated NF-κB activation and inflammation

- DA-DRD5 signaling can protect mice against *S. aureus*-induced sepsis and meningitis

Authors

Yuqing Wu, Yingchao Hu, Bingwei Wang, ..., Paul N. Moynagh, Jiawei Zhou, Shuo Yang

Correspondence

bingweiwang@njucm.edu.cn (B.W.), shuoyang@njmu.edu.cn (S.Y.)

In Brief

Wu et al. demonstrate that, upon DA-DRD5 signaling activation, the DRD5 receptor can directly recruit TRAF6 and its negative regulator ARRB2 to form a multi-protein complex also containing downstream signaling proteins, such as IKKs and PP2A, that impairs TRAF6-mediated activation of NF-κB and inflammation during acute *S. aureus* infection.

CellPress

Dopamine Uses the DRD5-ARRB2-PP2A Signaling Axis to Block the TRAF6-Mediated NF-κB Pathway and Suppress Systemic Inflammation

Yuqing Wu,[1,6] Yingchao Hu,[1,6] Bingwei Wang,[2,6,*] Sheng Li,[1] Chunmei Ma,[1] Xue Liu,[1] Paul N. Moynagh,[3,4] Jiawei Zhou,[5] and Shuo Yang[1,7,*]

[1]Department of Immunology, Key Laboratory of Immunological Environment and Disease, State Key Laboratory of Reproductive Medicine, Center for Global Health, Nanjing Medical University, Nanjing, China
[2]Department of Pharmacology, Nanjing University of Chinese Medicine, Nanjing, China
[3]Kathleen Lonsdale Institute for Human Health Research, Department of Biology, National University of Ireland Maynooth, Maynooth, Ireland
[4]Wellcome-Wolfson Institute for Experimental Medicine, Queen's University Belfast, Belfast, UK
[5]Institute of Neuroscience, State Key Laboratory of Neuroscience, Shanghai Institutes for Biological Sciences, Chinese Academy of Sciences, Shanghai, China
[6]These authors contributed equally
[7]Lead Contact
*Correspondence: bingweiwang@njucm.edu.cn (B.W.), shuoyang@njmu.edu.cn (S.Y.)
https://doi.org/10.1016/j.molcel.2020.01.022

SUMMARY

The functional relevance and mechanistic basis of the effects of the neurotransmitter dopamine (DA) on inflammation remain unclear. Here we reveal that DA inhibited TLR2-induced NF-κB activation and inflammation via the DRD5 receptor in macrophages. We found that the DRD5 receptor, via the EFD and IYX(X)I/L motifs in its CT and IC3 loop, respectively, can directly recruit TRAF6 and its negative regulator ARRB2 to form a multi-protein complex also containing downstream signaling proteins, such as TAK1, IKKs, and PP2A, that impairs TRAF6-mediated activation of NF-κB and expression of pro-inflammatory genes. Furthermore, the DA-DRD5-ARRB2-PP2A signaling axis can prevent *S. aureus*-induced inflammation and protect mice against *S. aureus*-induced sepsis and meningitis after DA treatment. Collectively, these findings provide the first demonstration of DA-DRD5 signaling acting to control inflammation and a detailed delineation of the underlying mechanism and identify the DRD5-ARRB2-PP2A axis as a potential target for future therapy of inflammation-associated diseases such as meningitis and sepsis.

INTRODUCTION

Innate immune cells, such as macrophages, dendritic cells, and neutrophils, mediate responses to pathogen-associated molecular patterns (PAMPs) or damage-associated molecular patterns (DAMPs) via their pattern recognition receptors (PRRs) and are pivotal in initiating inflammation in response to infection or sterile injury (Chen and Nuñez, 2010; Takeuchi and Akira, 2010). PRR-mediated innate immune cell activation recruits a plethora of downstream signal transducers, including adaptor proteins (MyD88, TRIF, MAVS, and STING; Liu et al., 2015; Yamamoto et al., 2003), kinases (IRAK, RIP, TAK1, TBK1, and IKKs; Kawai and Akira, 2007), and ubiquitin ligases (TRAF6, TRAF3, cIAP, ITCH, and Pellino; Jiang and Chen, 2011), to trigger intracellular signaling, which leads to activation of transcription factors, including nuclear factor κB (NF-κB), AP-1, and interferon regulatory factors (IRFs), enhancing transcription of targeted genes encoding proinflammatory cytokines and chemokines, interferons, and other inflammatory modulators (Hayden and Ghosh, 2012). However, the inflammatory response needs to be tightly controlled and resolved in a timely manner because excessive and persistent inflammation can cause lethal and diverse inflammatory diseases, including sepsis, atherosclerosis, inflammatory bowel disease, neurodegenerative disease, and systemic lupus erythematosus (Medzhitov, 2008).

Interestingly, recent progress in understanding physiological mechanisms that control inflammation has identified a regulatory connection between the nervous and immune systems. The studies indicate that stimulation of the vagus nerve prevents lethal experimental sepsis by controlling systemic inflammation (Borovikova et al., 2000). Previous studies indicate that cholinergic and catecholaminergic signaling play critical roles in mediating neuroimmune regulation in inflammatory diseases, including sepsis, inflammatory bowel disease, and arthritis (Nakai et al., 2014; Pavlov et al., 2018; Rosas-Ballina and Tracey, 2009), suggesting a vital role of neural regulation in peripheral inflammation.

Dopamine (DA) is an important member of catecholaminergic neurotransmitters that control movement, reward-seeking behavior, motivation, and cognition (Nieoullon, 2002). DA is produced not only in the central and peripheral nervous system but also by chromaffin cells of the suprarenal gland, epithelial cells in the gut, and peripheral immune cells (Daubner et al., 2011; Pacheco et al., 2014). DA exerts widespread effects by acting on DA receptors (DRs), which are divided into two primary
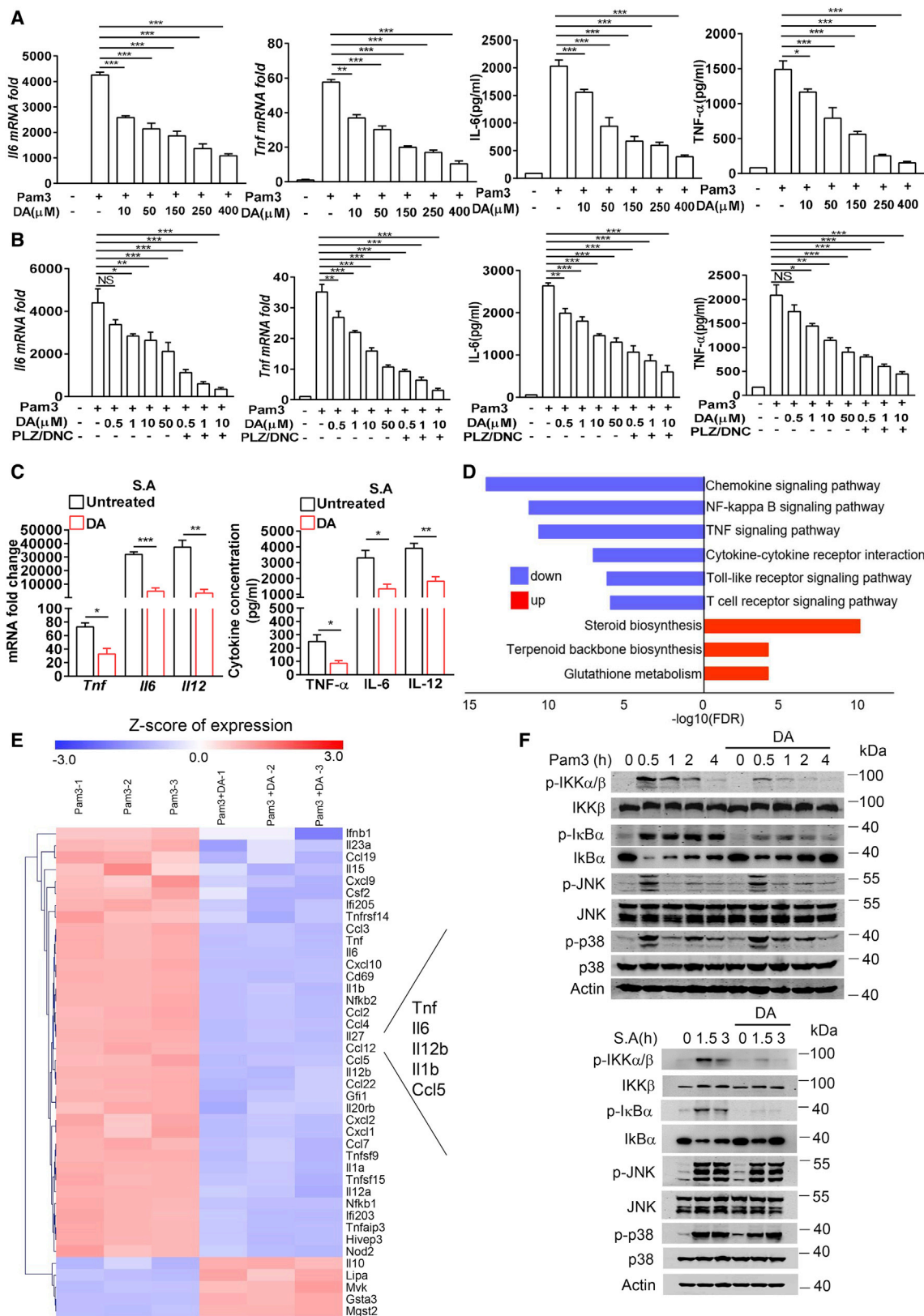
(legend on next page)

subfamilies: D1-like DRs that comprises DRD1 and DRD5, and D2-like DRs consisting of DRD2, DRD3, and DRD4 (Beaulieu et al., 2005). To date, DA has been reported to modulate the activation and chemotaxis of different immune cells by acting on its receptors and so act as an important regulator of the immune system (Pacheco et al., 2014). A previous study demonstrated that DRD2 activation in astrocytes can suppress neuroinflammation in the central nervous system via αB-crystallin (Shao et al., 2013). A recent study reported that follicular helper T (TFH) cell-derived DA activates DRD1 on germinal center B cells to enhance T-B cell interactions (Papa et al., 2017). Moreover, DA, via DRD1 signaling, specifically inhibits NLRP3 inflammasome activation and related inflammation (Yan et al., 2015). However, another study reported that DA induced by electrical stimulation of the vagus nerve can more generally inhibit the production of various cytokines, such as tumor necrosis factor (TNF), MCP-1, interleukin-6 (IL-6), and interferon-γ (IFN-γ), via D1-like receptors and control sepsis (Torres-Rosas et al., 2014). Thus, the molecular and mechanistic bases of DA-DRD signaling controlling systemic inflammation remains to be defined.

Here we identify, for the first time, that DA activates DRD5 to directly recruit the negative regulators ARRB2 and protein phosphatase 2A (PP2A) into the TRAF6-IKK complex in TLR2 signaling and so prevent S. aureus-induced systemic inflammation and neuroinflammation after DA treatment.

RESULTS

DA Inhibits TLR2-Induced Inflammation and NF-κB Activation

To investigate the wider role of DA in controlling inflammation, we treated bone marrow-derived macrophages (BMDMs) with Pam3CSK4 (Pam3), a TLR2 ligand that is a potent activator of inflammatory pathways and can induce inflammasome-independent inflammation (Ozinsky et al., 2000). We found that DA treatment significantly inhibited Pam3-induced expression of cytokines such as IL-6 and TNF-α at the mRNA and protein levels in a dose-dependent manner (Figures 1A and 1B). Consistent with previous reports showing that DA is subject to degradation by monoamine oxidase (MAO) and catechol-O-methyltransferase (COMT) to shorten its half-life (Yan et al., 2015; Youdim et al., 2006), we found that co-treatment with MAO and COMT inhibitors can greatly improve the DA inhibitory effect on Pam3-

induced IL-6 and TNF-α expression even at the lowest DA concentration of 0.5 μM (Figure 1B). These results again highlight the anti-inflammatory effects of DA and suggest that this effect extends beyond the mere ability to inhibit the NLRP3 inflammasome. Staphylococcus aureus (S. aureus) is a Gram-positive (G⁺) bacterium and can be recognized by TLR2 to activate TLR2-mediated inflammation (Oliveira-Nascimento et al., 2012). Therefore, we next investigated whether DA could restrict the production of proinflammatory cytokines during live S. aureus infection. Similar to inhibition of Pam3-induced inflammation, DA markedly inhibited production of IL-6, TNF-α, and IL-12 in S. aureus-infected BMDMs (Figure 1C). Taken together, these results clearly demonstrate that DA inhibits TLR2-induced inflammatory responses in macrophages.

Next we probed the mechanism by which DA can inhibit TLR2-induced inflammation. First we performed RNA sequencing (RNA-seq) to analyze the transcriptional profiles of Pam3-stimulated BMDMs treated in the absence or presence of DA. Interestingly, Kyoto Encyclopedia of Genes and Genomes (KEGG) analysis showed that one of the most prominent downregulated pathways upon DA treatment was the NF-κB signaling pathway (Figure 1D). Consistently, the heatmap analysis displayed a significant decrease in expression of a variety of genes associated with NF-κB signaling and inflammation, such as Il6, Tnf, Il12b, Il1b, and Ccl5 (Figure 1E). We further found that DA remarkably reduced the capacity of Pam3 or S. aureus to induce phosphorylation of IKKs or of their substrate IκBα, both of which are activation indices of the canonical NF-κB pathway (Figure 1F). Moreover, IκBα degradation after stimulation with Pam3 or S. aureus infection was significantly impaired in the presence of DA. In contrast, DA did not affect the ability of Pam3 or S. aureus to promote phosphorylation of JNK or p38, major components of the mitogen-activated protein kinase (MAPK) signaling pathway (Figure 1F). Notably, DA inhibited nuclear accumulation of the NF-κB subunit p65 in Pam3-stimulated BMDMs (Figure S1). Taken together, these data suggest that DA specifically inhibits TLR2-mediated NF-κB signaling and subsequent inflammation.

DA Inhibits TLR2-Induced Inflammation via DRD5

To determine which DR subtype mediates the inhibitory effect of DA on TLR2-induced inflammation, we first measured the expression of DRs in BMDMs after Pam3 stimulation or

---

Figure 1. Dopamine Inhibits TLR2-Induced Inflammation and NF-κB Activation

(A) Left: qRT-PCR analysis of Il6 and Tnf mRNA expression in BMDMs treated with various doses of DA and stimulated with Pam3CSK4 (Pam3; 2 μg/mL) for 6 h. Right: ELISA of IL-6 and TNF-α in supernatants from BMDMs treated as indicated for 18 h.

(B) Left: qRT-PCR analysis of Il6 and Tnf mRNA expression in BMDMs treated with phenelzine (PLZ, 10 μM) plus 3,5-dinitrocatechol (DNC, 10 μM) and different doses of DA and stimulated with Pam3 for 6 h. Right: ELISA of IL-6 and TNF-α in supernatants from BMDMs treated as indicated for 18 h.

(C) qRT-PCR analysis of Il6, Tnf, and Il12 mRNA expression in BMDMs treated with DA (150 μM) and infected with S. aureus (MOI = 10) for 6 h and ELISA analysis of IL-6, TNF-α, and IL-12 in supernatants from BMDMs treated as indicated for 18 h.

(D) KEGG analysis of the most significantly altered signaling pathways in Pam3-stimulated BMDMs left untreated or treated with DA 6 h after stimulation.

(E) Heatmap of genes with an adjusted false discovery rate (FDR) of less than 0.001 and log2 fold change of more than 2 from RNA-seq analysis of Pam3-stimulated BMDMs left untreated or treated with DA.

(F) Immunoblot analysis of phosphorylated (p-) and total IKKα/β, IκBα, JNK, and p38 in lysates of BMDMs treated with DA (150 μM) and stimulated with Pam3 (2 μg/mL) or S. aureus infection (MOI = 10).

Data are pooled from three independent experiments (A–C) or representative of three independent experiments (F). Error bars show means ± SEM. *p < 0.05, **p < 0.01, ***p < 0.001; NS, not significant. One-way ANOVA with Dunnett's multiple comparisons test for (A) and (B) and unpaired t test for (C).

See also Figure S1.
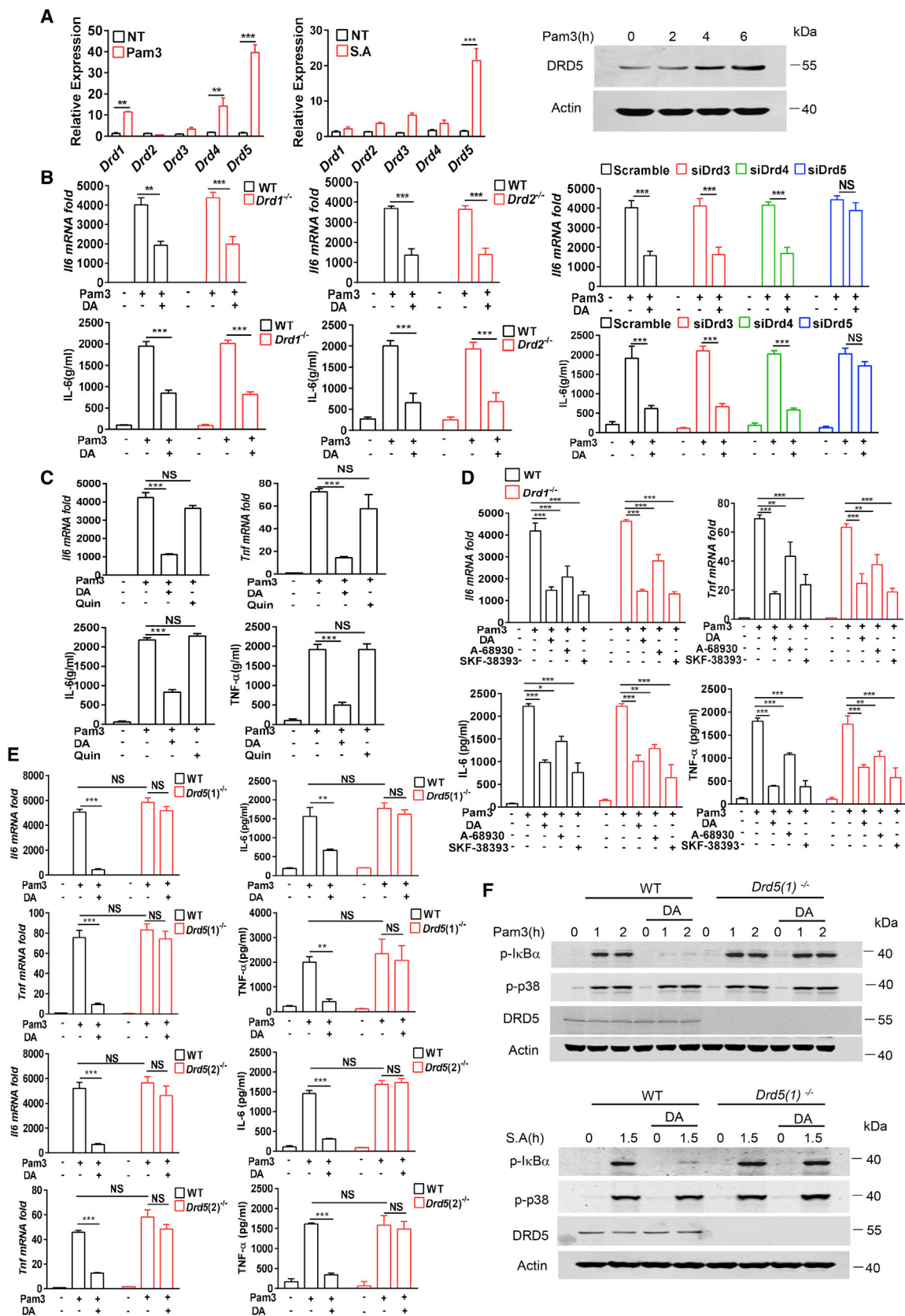
S. aureus infection. Interestingly, we observed that DRD5 was unique because its expression in BMDMs was significantly increased in response to Pam3 treatment or *S. aureus* infection, whereas the expression levels of other DRDs were not markedly regulated (Figure 2A). Likewise, the public datasets showed that gene expression of DRD5, but not other DRDs, was significantly increased in PBMCs from *S. aureus*-infected patients (GSE26378 and GSE54514) (Figure S2A). To further determine which DRD subtype was involved in the anti-inflammatory effect of DA, we next screened the potential role of each of the 5 DRD subtypes by using DRD1 and DRD2 knockout BMDMs and DRD3, DRD4, and DRD5 small interfering RNA (siRNA) knockdown BMDMs. The results showed that knockdown of *Drd5* in BMDMs greatly suppressed the inhibitory effect of DA on TLR2-induced IL-6 and TNF-α production, whereas knockout of *Drd1* and *Drd2* and knockdown of *Drd3* and *Drd4* had no effect (Figure 2B; Figures S2B and S2C). In addition, the D2-like agonist quinpirole did not inhibit Pam3-induced expression of IL-6 and TNF-α in wild-type (WT) BMDMs, whereas, similar to DA, the selective D1-like agonists A-68930 and SKF-38393 markedly reduced production of IL-6 and TNF-α in response to Pam3, even in *Drd1*$^{-/-}$ BMDMs (Figures 2C and 2D). Notably, SKF-38393, which has a higher affinity for the D5 receptor, exhibited stronger inhibitory effects on the production of proinflammatory cytokines than A-68930 (Figure 2D). To further confirm that DA exerts its anti-inflammatory effects through DRD5, we generated two different *Drd5*$^{-/-}$ mouse lines by using the CRISPR-Cas9 system, and both knockout mice developed normally (Figure S2D). As expected, the inhibitory effect of DA on the expression of IL-6 and TNF-α in response to Pam3 was completely lost in BMDMs from both *Drd5*$^{-/-}$ lines (Figure 2E). Moreover, loss of phosphorylation of IκBα by DA was observed in WT but not *Drd5*$^{-/-}$ BMDMs after stimulation with Pam3 or *S. aureus* infection (Figure 2F). Collectively, these results clearly demonstrate that DA inhibits TLR2-induced inflammation specifically via DRD5.

DA Inhibits TRAF6-Dependent Inflammation Independently of Cyclic AMP (cAMP)-Protein Kinase A (PKA) Signaling

Next, we set out to determine how DA-DRD5 signaling inhibits TLR2-induced NF-κB activation and pro-inflammatory gene expression. D1-like signaling can couple to Gαs, which enhances cAMP accumulation and activation of PKA (Beaulieu and Gainetdinov, 2011). We found that inhibition of PKA with H89 or a reduction in cAMP levels with the adenylate cyclase (ADCY) inhibitor KH7 did not reverse DA-mediated inhibition of IL-6 and TNF-α production induced by Pam3. Moreover, H89 or KH7 treatment did not affect loss of Pam3-induced phosphorylation of IKKs and IκBα in the presence of DA (Figure 3A). These results suggest that cAMP-PKA signaling is not required for the inhibitory effect of DA on TLR2-induced inflammation and NF-κB activation.

Mammalian Toll-like receptors (TLRs) can recognize PAMPs in pathogens to trigger downstream activation of NF-κB and then induce transcription of genes encoding proinflammatory cytokines. TLR signaling pathways can be divided into MyD88-dependent pathways, which are common to all TLRs except for TLR3, and MyD88-independent pathways, which are particular to the TLR3 and partial TLR4 signaling pathways (Takeda and Akira, 2004). To determine the sensitivities of these different pathways to the inhibitory effect of DA, we assessed the effect of DA on pro-inflammatory cytokine production and phosphorylation of IKKs in BMDMs treated with a wide array of ligands for TLR2, TLR3, TLR4, TLR5, TLR7/8, and TLR9. Interestingly, we observed that DA can inhibit expression of IL-6 and TNF-α and phosphorylation of IKKs induced by all TLR ligands, except the TLR3 agonist poly(I:C) (Figures 3B and 3C). This result suggests that DA specially inhibits the MyD88-dependent arm of TLR pathways and downstream TRAF6-mediated NF-κB inflammatory signaling.

DRD5 Utilizes the IYX(X)I/L Motif of Its Third Intracellular Loop (IC3) and the EFD Motif of Its C-Terminal Tail (CT) to Recruit ARRB2 and TRAF6, Respectively, and Form DRD5/ARRB2/TRAF6 Protein Complexes

It is known that activation of DRs can recruit the scaffolding protein ARRB2 to desensitize DRD and that ARRB2 can negatively regulate TRAF6 signaling (Beaulieu et al., 2005; Luttrell and Lefkowitz, 2002; Wang et al., 2006); therefore, we speculated that DRD5 may use ARRB2 to directly block TRAF6 downstream signaling and induction of pro-inflammatory cytokines. To test this possibility, we initially assessed the ability of DRDs to interact with TRAF6. Coimmunoprecipitation analysis of

---

Figure 2. Dopamine Inhibits TLR2-Induced Inflammation via DRD5

(A) qRT-PCR analysis of *Drd1*, *Drd2*, *Drd3*, *Drd4*, and *Drd5* mRNA expression in BMDMs after Pam3 stimulation or *S. aureus* infection for 6 h and immunoblot analysis of DRD5 protein expression in BMDMs treated with Pam3 as indicated.

(B) Top: qRT-PCR analysis of *Il6* mRNA expression in WT, *Drd1*$^{-/-}$, *Drd2*$^{-/-}$, control (scramble), Drd3, Drd4, and Drd5 siRNA knockdown BMDMs treated as indicated for 6 h. Bottom: ELISA of IL-6 in supernatants from WT, *Drd1*$^{-/-}$, *Drd2*$^{-/-}$, control, Drd3, Drd4, and Drd5 siRNA knockdown BMDMs treated as indicated for 18 h.

(C) Top: RT-PCR analysis of *Il6* and *Tnf* mRNA expression in BMDMs treated with quinpirole (Quin, 20 μM) or DA and stimulated with Pam3 for 6 h. Bottom: ELISA of IL-6 and TNF-α in supernatants from BMDMs treated as indicated for 18 h.

(D) Top: RT-PCR analysis of *Il6* and *Tnf* mRNA expression in WT and *Drd1*$^{-/-}$ BMDMs treated with DA, A-68930, or SKF-38393 (20 μM) and stimulated with Pam3 for 6 h. Bottom: ELISA of IL-6 and TNF-α in supernatants from WT and *Drd1*$^{-/-}$ BMDMs treated as indicated for 18 h.

(E) Left: qRT-PCR analysis of *Il6* and *Tnf* mRNA expression in WT, *Drd5*(1)$^{-/-}$, and *Drd5*(2)$^{-/-}$ BMDMs treated as indicated for 6 h. Right: ELISA of IL-6 and TNF-α in supernatants from WT, *Drd5*(1)$^{-/-}$, and *Drd5*(2)$^{-/-}$ BMDMs treated as indicated for 18 h.

(F) Immunoblot analysis of p-IκBα, p-p38, and DRD5 in lysates of WT and *Drd5*$^{-/-}$ BMDMs treated as indicated.

Data are pooled from three independent experiments (A–D) or representative of three independent experiments (F). Error bars show means ± SEM. *p < 0.05, **p < 0.01, ***p < 0.001; NS, not significant. Two-way ANOVA with Sidak's multiple comparisons test for (A)–(E).
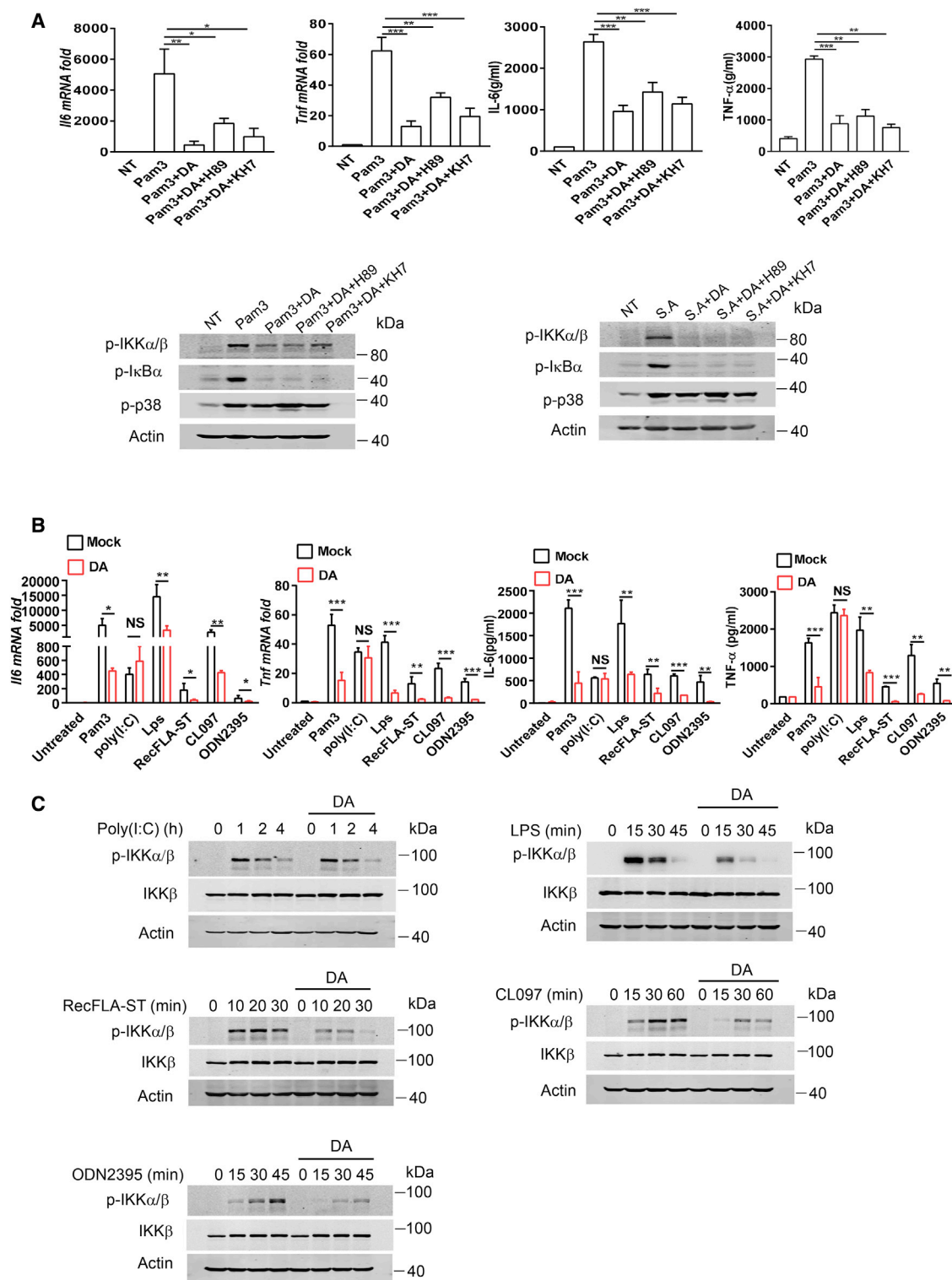
See also Figure S2.

Figure 3. Dopamine Inhibits TRAF6-Dependent Inflammation Independent of cAMP-PKA Signaling

(A) Top left: qRT-PCR analysis of *Il6* and *Tnf* mRNA expression in BMDMs treated with DA and H89 (40 μM) or KH7 (5 μM) and stimulated with Pam3 for 6 h. Top right: ELISA of IL-6 and TNF-α in supernatants from BMDMs treated as indicated for 18 h. Bottom: immunoblot analysis of p-IKKα/β, p-IκBα, and p-p38 in lysates of BMDMs treated as indicated.

(legend continued on next page)

transfected cells with C terminus Myc-tagged human DRDs and FLAG-tagged human TRAF6, using an anti-Myc antibody to immunoprecipitate DRDs, demonstrated that TRAF6 was co-precipitated with DRD1, DRD3, and DRD5 (Figure 4A). Notably, the electrophoretic mobility of DRD proteins tended to manifest as broad smears spanning molecular weight ranges of more than 60–120 kDa. Such heterogeneity in size likely represents various glycosylated forms of overexpressed DRDs, as reported previously (Free et al., 2007). Moreover, consistent with previous studies, immunoprecipitation assays indicated that ARRB2 interacted with all DRDs (Figure 4B). We next investigated whether DRD5 can associate with TRAF6 and ARRB2 to form a multi-protein complex while also assessing whether DRD1 and DRD3 can. We observed that interaction of DRD1 or DRD3 with ARRB2 was severely impaired when co-expressed with TRAF6 but interaction between DRD5 and ARRB2 was not. Additionally, association of DRD1 or DRD3 with TRAF6 was greatly inhibited in the presence of ARRB2 co-expression, whereas DRD5 interaction with TRAF6 was normal (Figure 4C). These data suggest that only DRD5, ARRB2, and TRAF6 can coexist in the same protein complex.

DRs contain 3 intracellular loops (IC1–IC3), 3 extracellular loops (EC1–EC3), and an extracellular amino terminus and cytoplasmic C-terminal tail (CT) (Beaulieu and Gainetdinov, 2011). IC3 and the cytoplasmic CT of DA receptors are the major cytoplasmic regions responsible for protein interactions and signal transduction after DRD activation (Neve et al., 2004). D1-like receptors are significantly longer in their CTs compared with D2-like receptors. In contrast, D2-like receptors are characterized by a long IC3 (Missale et al., 1998). A previous study indicated that the IYIVL sequence at the N terminus of IC3 of DRD2 is a key element of the arrestin binding site (Lan et al., 2009). Amino acid sequence alignment revealed that the N terminus of IC3 of human DRD1, DRD3, and DRD5 includes the IYX(X)I/L (X is any amino acid) motif, which may be a putative high-affinity binding site for ARRB2. We therefore performed alanine substitution on the IYX(X)I/L motifs of DRD1, DRD3, and DRD5 and generated the substitution mutants hD1Am, hD3Am, and hD5Am (Figure 4D). Coimmunoprecipitation analysis showed that the IYX(X)I/L substitution mutation in IC3 blocked interaction of DRD1, DRD3, and DRD5 with ARRB2 (Figure 4D), suggesting an essential role of the IYX(X)I/L motif of DRDs in the interaction with ARRB2.

Next, we sought to investigate the regions required for TRAF6 interacting in DRD1, DRD3, and DRD5. We generated several IC3 and CT region deletion mutants of DRD1, DRD3, and DRD5 (including hD1IC3 dm, hD1CTdm, hD3IC3dm, and hD5CTdm) and then conducted TRAF6 interaction studies by coimmunoprecipitation experiments. Deletion of IC3 but not the CT region of DRD1 abolished its interaction with TRAF6 (Figure 4E). Moreover, deletion of the DRD3 IC3 region disrupted

TRAF6 interaction (Figure 4F). For DRD5, deletion of the CT region could completely inhibit its interaction with TRAF6 (Figure 4G). These results suggest that DRD1 and DRD3 utilize IC3, whereas DRD5 utilizes CT as a TRAF6-interacting region. Thus, unlike DRD5, the TRAF6- and ARRB2-interacting regions in DRD1 and DRD3 overlap, which could explain why DRD1 and DRD3 cannot form protein complexes with ARRB2 and TRAF6 but DRD5 can (Figure S3).

A previous study identified P-X-E-X-X-Ar/Ac (where Ar is an aromatic and Ac is an acidic residue) sequence as a TRAF6-binding motif (Ye et al., 2002). Although the human DRD5 CT region lacks this canonical binding motif, a closely related motif, rich in Ac and Ar amino acids at 424–435 of the DRD5 CT (EVDNDEEEGPFD) was observed (Figure 4G). Sequence alignment of DRD5 from several other mammalian species revealed that these CT residues of DRD5 are highly conserved (Figure 5A). Hereafter, we refer to this Ac/Ar-rich region as the EFD motif. Next, we generated the DRD5 EFD motif mutant hD5EFDm, in which the Ac and Ar amino acids of the EFD motif were substituted with alanine. Interestingly, coimmunoprecipitation experiments showed that the EFD motif mutation disrupted interaction of DRD5 with TRAF6 (Figure 4G), suggesting that the interaction DRD5 with TRAF6 was facilitated via the EFD motif in the CT of DRD5.

Because the EFD and IYX(X)I/L motifs of DRD5 are highly conserved in different species (Figure 5A), we next extended these findings to murine counterparts. Consistent with the human findings, CT deletion and EFD motif mutation disrupted mouse DRD5 interaction with mouse TRAF6 (Figure 5B). Moreover, the IYX(X)I/L substitution mutation in IC3 abolished mouse DRD5 interaction with ARRB2 (Figure 5C). As a control, we found that IC3 deletion and IYX(X)I/L mutation of IC3 in mouse DRD1 abolished its TRAF6 and ARRB2 interaction, respectively (Figures 5B and 5C). These data suggest a conserved mechanism across species for DRD5 interaction with TRAF6 and ARRB2. We also conducted an in vitro glutathione S-transferase (GST) pull-down assay. GST fusion proteins containing the mouse DRD1 CT (mD1CT), mouse DRD5 CT (mD5CT), and mouse DRD5 CT EFD mutant (mD5CTEFDm) were purified and used as bait to precipitate associated proteins. We observed that GST-mD5CT, but not GST-mD5CTEFDm, GST-mD1CT, or GST alone, was able to pull down TRAF6 from protein extracts prepared from Pam3-treated BMDMs (Figure 5D), further indicating an interaction between DRD5 and endogenous TRAF6 via the EFD motif.

To directly characterize the association of DRD5 with ARRB2 and TRAF6 in more physiologically relevant settings, we also examined the interaction of DRD5 with ARRB2 and TRAF6 in BMDMs in response to Pam3, DA, or Pam3/DA co-treatment using coimmunoprecipitation experiments. The studies showed that DA only induced interaction of DRD5 with ARRB2 and its

(B) Left and center left: qRT-PCR analysis of *Il6* and *Tnf* mRNA expression in BMDMs treated with DA (150 μM) and stimulated with Pam3 (2 μg/mL), poly(I:C) (50 μg/mL), lipopolysaccharide (LPS; 200 ng/mL), recombinant flagellin from *Salmonella typhimurium* (RecFLA-ST; 50 ng/mL), CL097 (2 μg/mL), and ODN2395(1 μM) for 6 h. Right and center right: ELISA of IL-6 and TNF-α in supernatants from BMDMs treated as indicated for 18 h.

(C) Immunoblot analysis of phosphorylated and total IKKα/β in lysates of BMDMs treated as indicated.

Data are pooled from three independent experiments (A and B) or representative of two independent experiments (C). Error bars show means ± SEM. *p < 0.05, **p < 0.01, ***p < 0.001; NS, not significant. One-way ANOVA with Dunnett's multiple comparisons test for (A) and unpaired t test for (B).
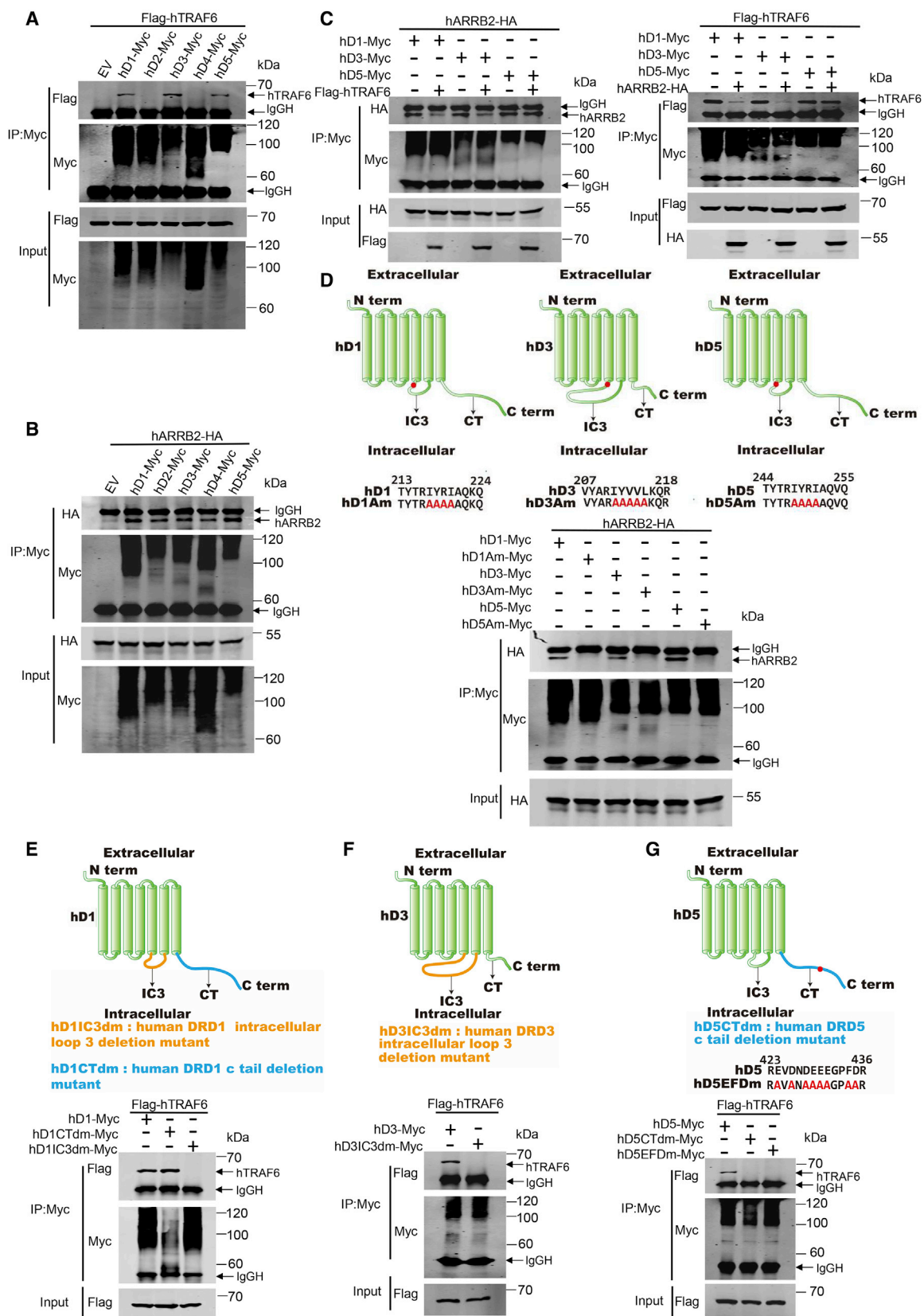
(legend on next page)

downstream effector PP2A, whereas Pam3 plus DA treatment led to interaction of DRD5 with ARRB2, PP2A, TRAF6, and kinases downstream of TRAF6, including TAK1 and IKKβ. However, treatment with Pam3 and DA failed to induce interaction of DRD5 with the MAPK p38 (Figure 5E). As reported, TRAF6 dissociates from TLRs and then forms signaling complexes with other proteins, such as TAK1 and IKKs, after activation by IRAK-1 in TLR signaling (Takeda and Akira, 2004). Thus, our results suggest that, upon activation by DA and Pam3, DRD5 can recruit ARRB2, TRAF6, and their downstream effectors to form a multi-protein complex and that this may underlie the negative regulation of the NF-κB pathway by DA.

Inhibition of TLR2-Induced Inflammation by DRD5 Activation Requires the ARRB2/PP2A Signaling Complex

To further determine whether ARRB2 participates in DA-mediated negative regulation in TLR2-induced inflammation, we analyzed Pam3- or *S. aureus*-induced expression of IL-6 and TNF-α in WT and *Arrb2*$^{-/-}$ BMDMs in the presence or absence of DA. The results showed that DA treatment inhibited IL-6 and TNF-α production in WT BMDMs in response to Pam3 stimulation or *S. aureus* infection, but such inhibitory effects of DA were severely impaired in *Arrb2*$^{-/-}$ cells (Figure 6A). Moreover, inhibition of phosphorylation of IκBα by DA was lost in *Arrb2*$^{-/-}$ BMDMs after Pam3 stimulation or *S. aureus* infection (Figure 6B).

Given that ARRB2 can form a signaling complex with PP2A in response to DA receptor activation and that PP2A has been shown to negatively regulate NF-κB signaling through dephosphorylation of IKKβ (Beaulieu et al., 2005; Witt et al., 2009), we next investigated the potential role of PP2A in mediating the anti-inflammatory effects of DA. We crossed PP2A core enzyme C subunit floxed mice with *LysM*-Cre mice to generate myeloid-specific conditional knockout mice (*PP2Ac*$^{f/f}$*LysM*-Cre) and then isolated BMDMs from these mice to assess the effect of PP2A

deficiency on the anti-inflammatory effects of DA. In contrast to *PP2Ac*$^{f/f}$ control cells, inhibition of Pam3- or *S. aureus*-induced expression of IL-6 and TNF-α by DA was greatly impaired in *PP2Ac*$^{f/f}$*LysM*-Cre BMDMs (Figure 6C). PP2A-deficient cells were also resistant to the inhibitory effects of DA on Pam3- and *S. aureus*-induced phosphorylation of IκBα (Figure 6D). Moreover, PP2A inhibition by okadaic acid (OA) precluded the inhibitory effect of DA on TLR2-induced inflammation and NF-κB activation (Figure S4A). NF-κB luciferase reporter assays further showed that transfection of DRD5, ARRB2, and PP2Ac, but not other DRDs, can suppress TRAF6-induced expression of the luciferase reporter in HEK293T cells (Figure S4B).

Because ARRB2 interacts with TRAF6 after TLR activation to negatively regulate TLR signaling (Wang et al., 2006), we next evaluated whether DA facilitated Pam3-induced interaction of ARRB2 and PP2A with TRAF6 in WT and *Drd5*$^{-/-}$ BMDMs. We found that DA and Pam3 strongly promoted recruitment of ARRB2 and PP2A to TRAF6 in WT BMDMs, but this was abrogated in *Drd5*$^{-/-}$ cells (Figure 6E). Moreover, a coimmunoprecipitation assay in HEK293T cells also indicated that DRD5 was able to promote interaction of ARRB2 with TRAF6 (Figure S4C). All of these data suggest that recruitment of the ARRB2/PP2A signaling complex to TRAF6 is necessary for mediating the anti-inflammatory effects of DA/DRD5 on the TLR2 pathway.

Inhibition of TLR2-Induced Inflammation by DRD5 Activation Depends on the Motifs of DRD5 Necessary for ARRB2 and TRAF6 Interaction

To further determine the functional roles of the IYX(X)I/L and EFD motifs of DRD5 in the inhibitory effects of DA on NF-κB activation, we conducted NF-κB luciferase reporter assays using D5Am and D5EFDm mutants. We found that mutations of the IYX(X)I/L and EFD motifs of DRD5 disrupted the inhibitory effects of DRD5 on induction of NF-κB-regulated reporter activity by

Figure 4. DRD5 Utilizes the IYX(X)I/L Motif of Its Third Intracellular Loop (IC3) and the EFD Motif of the C-Terminal Tail (CT) to Directly Interact with ARRB2 and TRAF6, Respectively

(A) Immunoblot analysis of FLAG (TRAF6) and Myc (DRD1–DRD5) proteins in immunoprecipitated Myc and lysate (input) samples from HEK293T cells transfected with constructs encoding FLAG-tagged human TRAF6 and Myc-tagged human DRDs (hD1–hD5).

(B) Immunoblot analysis of HA (ARRB2) and Myc (DRD1–DRD5) proteins in immunoprecipitated Myc and input samples from HEK293T cells transfected with constructs encoding hemagglutinin (HA)-tagged human ARRB2 and Myc-tagged human DRDs.

(C) Left: immunoblot analysis of coimmunoprecipitation of HA (ARRB2) and Myc (DRD1, DRD3, and DRD5) in the presence or absence of FLAG-tagged TRAF6 overexpression in HEK293T cells. Right: immunoblot analysis of coimmunoprecipitation of FLAG (TRAF6) and Myc (DRD1, DRD3, and DRD5) in the presence or absence of HA-tagged ARRB2 overexpression in HEK293T cells.

(D) Schematic of IYX(X)I/L motif mutants of human DRD1, DRD3, and DRD5 (hD1Am, hD3Am, and hD5Am) and immunoblot analysis of HA (ARRB2) and Myc (DRD1, DRD3, and DRD5 and their mutants) proteins in immunoprecipitated Myc and input samples from HEK293T cells transfected with constructs encoding HA-tagged human ARRB2 and Myc-tagged human DRDs (hD1, hD3, and hD5) or their corresponding arrestin binding mutants (hD1Am, hD3Am, and hD5Am).

(E) Schematic of IC3 and CT deletion mutants of human DRD1 (hD1IC3dm and hD1CTdm) and immunoblot analysis of FLAG (TRAF6) and Myc (DRD1 and its mutants) proteins in immunoprecipitated Myc and input samples from HEK293T cells transfected with constructs encoding FLAG-tagged human TRAF6 and Myc-tagged human DRD1 (hD1) or corresponding mutants (hD1IC3dm and hD1CTdm).

(F) Schematic of IC3 deletion mutants of human DRD3 (hD3IC3dm) and immunoblot analysis of FLAG (TRAF6) and Myc (DRD3 and its mutant) proteins in immunoprecipitated Myc and input samples from HEK293T cells transfected with constructs encoding FLAG-tagged human TRAF6 and Myc-tagged human DRD3 (hD3) or the corresponding mutant (hD3IC3 dm).

(G) Schematic of CT deletion and EFD motif mutants of human DRD5 (hD5CTdm and hD5EFDm) and immunoblot analysis of FLAG (TRAF6) and Myc (DRD5 and its mutants) proteins in immunoprecipitated Myc and input samples from HEK293T cells transfected with constructs encoding FLAG-tagged human TRAF6 and Myc-tagged human DRD5 (hD5) or the corresponding mutants (hD5CTdm and hD5EFDm).

Data are representative of three experiments.

See also Figures S3 and S7.
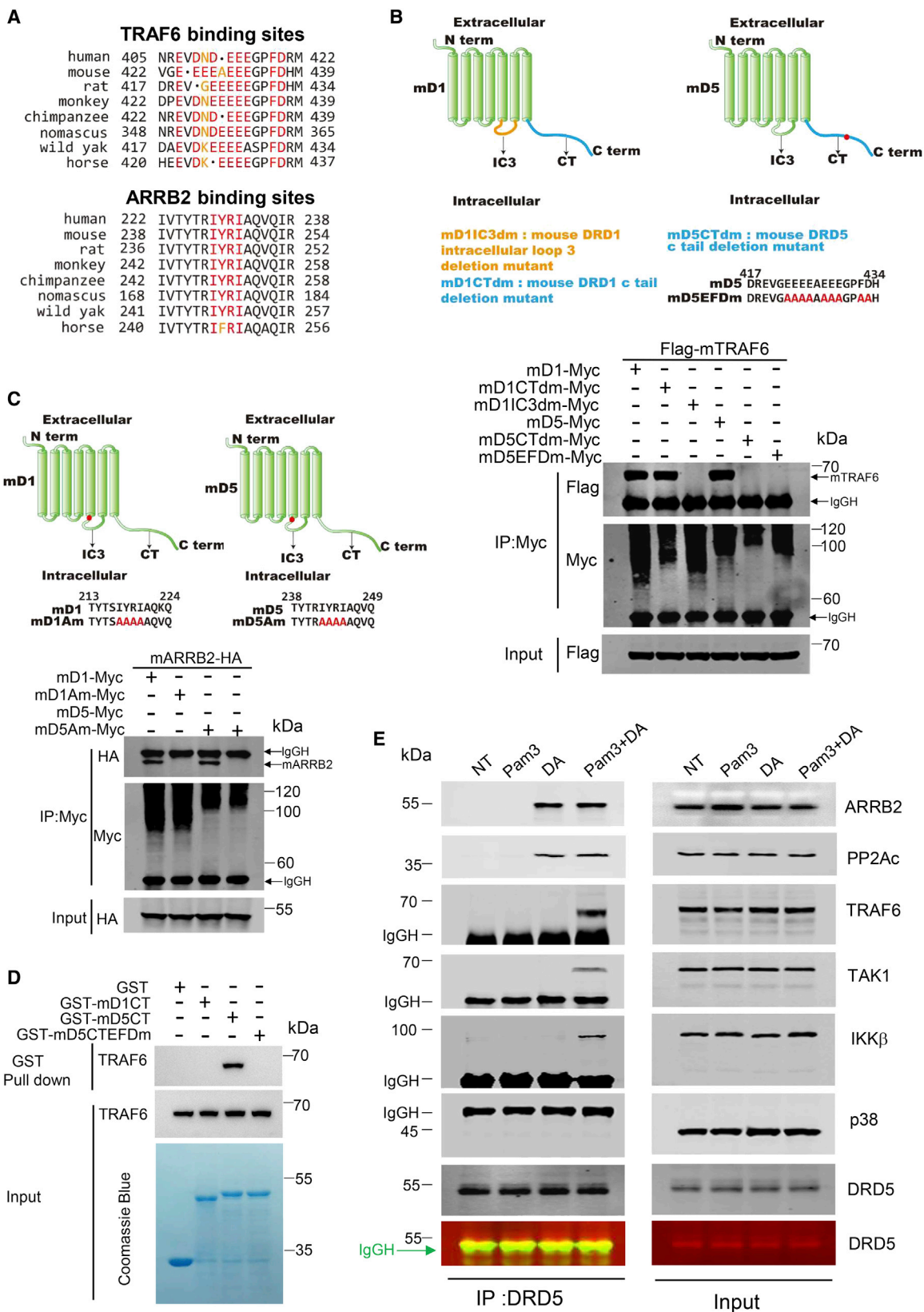
TRAF6 (Figure S5A). We further found that the deficiency in the inhibitory effect of DA on TLR2-induced expression of IL-6 and TNF-α in $Drd5^{-/-}$ BMDMs was rescued by reconstitution with WT mouse DRD5 but not the mutant forms of DRD5 containing mutations in the IYX(X)I/L or EFD motifs (Figure S5B). Moreover, the loss of inhibition of Pam3-induced phosphorylation of IκBα in DA-stimulated $Drd5^{-/-}$ BMDMs was rescued by reintroduction of WT mouse DRD5 but not by either of the mutated forms (Figure S5C). Altogether, these data indicate that ARRB2- and TRAF6-interacting motifs of DRD5 are key elements of the inhibitory effect of DA on TLR2-induced inflammation.

DRD5-ARRB2-PP2A Signaling Activation Prevents *S. aureus*-Induced Systemic Inflammation and Neuroinflammation after DA Treatment

Next we investigated whether DA could decrease production of inflammatory cytokines *in vivo* to protect against *S. aureus*-induced septic shock. To test this, we used an *S. aureus*-infected peritonitis mouse model. We intraperitoneally injected mice with a sublethal dose of *S. aureus* (ATCC 25923, 1×10^8 colony-forming units [CFUs]/mouse), simultaneously treated m with saline or DA (50 mg/kg of body weight), and then evaluated survival. We observed that *S. aureus* challenge resulted in about 75% lethality in both WT and $Drd5^{-/-}$ mice within 4 days, and DA treatment decreased the lethal rate to about 20% in WT mice but did not improve the survival of $Drd5^{-/-}$ mice. Moreover, *S. aureus* infection resulted in 100% lethality in $Arrb2^{-/-}$ and $PP2Ac^{f/f}LysM$-Cre mice within 4 days irrespective of DA administration (Figure 7A). The secretion of IL-6 and TNF-α in serum 12 h after infection with *S. aureus* was similar in WT and $Drd5^{-/-}$ mice and lower in DA-treated WT but not in $Drd5^{-/-}$ mice compared with untreated mice. Additionally, secretion of IL-6 and TNF-α was not changed significantly by DA treatment in $Arrb2^{-/-}$ and $PP2Ac^{f/f}LysM$-Cre mice. Furthermore, ARRB2 and PP2A deletion enhanced *S. aureus* infection-induced IL-6 and TNF-α production in mice (Figure 7B). $Drd5^{-/-}$ mice did not have a poorer outcome compared with WT animals when exposed to *S. aureus*, suggesting that endogenous DA did not limit inflammation via DRD5 in acute bacterial infection. We measured the endogenous DA concentration in blood or peripheral lymphoid organs, such as the spleen and draining lymph nodes, before and after *S. aureus* infection (24 h after infection). We found that the physiological concentration of DA in the periphery was $\sim 2 \times 10^{-8}$– 1.8×10^{-7} M (blood, $\sim 2 \times 10^{-8}$ M; spleen, $\sim 1.2 \times 10^{-7}$ M; lymph nodes, $\sim 1.8 \times 10^{-7}$ M). These concentrations of DA are close to the lowest concentration of DA (5×10^{-7}M) used in our *in vitro* studies, but, remarkably, *S. aureus* infection reduced the concentration of DA in the periphery to a range of $\sim 1 \times 10^{-9}$– 3×10^{-8} M (blood, $\sim 1 \times 10^{-9}$ M; spleen, $\sim 2.5 \times 10^{-8}$ M; lymph nodes, $\sim 3 \times 10^{-8}$ M), which is far lower than the dose response range in *in vitro* studies (Figure S6A). We speculate that such suppression of endogenous DA under conditions of infection may negate the potential anti-inflammatory effects of upregulation of DRD5 under the same conditions and so explain the comparable responses of WT and $Drd5^{-/-}$ mice to *S. aureus* infection. However, administration of exogenous DA presumably overcomes the effects of infection on the dopaminergic system to limit inflammation. Moreover, DA treatment tended to reduce the bacterial loads in the liver and peripheral lymphoid organs in WT mice 36 h after infection, but not in $Drd5^{-/-}$ mice (Figure S6B), suggesting that DA may reduce excessive inflammation via DRD5 during acute *S. aureus* infection to contribute to bacterial clearance. This is consistent with previous studies showing that, during acute systemic *S. aureus* infection, excessive inflammation can cause defective bacterial clearance and systemic dissemination of bacteria (Kitur et al., 2016; Leech et al., 2017).

S. aureus is a common cause of infection, causing life-threatening diseases such as meningitis (Tong et al., 2015). To test whether DA-DRD5 signaling is involved in controlling neuroinflammation induced by *S. aureus* infection, we used the *S. aureus*-induced meningitis mouse model and retro-orbital injection of *S. aureus* (ATCC 25923, 5×10^8 CFUs/mouse) and simultaneously treated mice with saline or the DRD5 agonist SKF-38393 (10 mg/kg of body weight). Fluorescence-activated cell sorting (FACS) analysis showed that SKF-38393 treatment could reduce the percentages and absolute numbers of activated microglia and peripheral myeloid cells (CD45^{high}CD11b$^+$) infiltrating the brain of WT mice after *S. aureus*-induced meningitis, whereas the inhibitory effects of SKF-38393 were severely impaired in $Drd5^{-/-}$, $Arrb2^{-/-}$, and $PP2Ac^{f/f}LysM$-Cre mice. Moreover, infiltration of CD45^{high}CD11b$^+$ cells in the brain after *S. aureus* infection was significantly increased in $Arrb2^{-/-}$ and $PP2Ac^{f/f}LysM$-Cre mice (Figure 7C). Consistent with FACS

Figure 5. DRD5 Utilizes the IYX(X)I/L Motif of Its IC3 and the EFD Motif of the CT to Directly Interact with ARRB2 and TRAF6, Respectively
(A) Alignment of the conserved EFD and IYX(X)I/L motifs of DRD5 in several mammalian species.
(B) Schematic of IC3 and CT deletion mutants of mouse DRD1 and CT deletion and EFD motif mutants of mouse DRD5 (mD1IC3dm, mD1CTdm, mD5CTdm, and mD5EFDm) and immunoblot analysis of FLAG (TRAF6) and Myc (DRD1, DRD5, and their mutants) proteins in IP Myc and input samples from HEK293T cells transfected with constructs encoding FLAG-tagged mouse TRAF6 and Myc-tagged mouse DRD1 and DRD5 (mD1 and mD5) or their corresponding mutants (mD1IC3dm, mD1CTdm, mD5CTdm, and mD5EFDm).
(C) Schematic of IYX(X)I/L motif mutants of mouse DRD1 and DRD5 (mD1Am and mD5Am) and immunoblot analysis of HA (ARRB2) and Myc (DRD1, DRD5, and their mutants) proteins in immunoprecipitated Myc and input samples from HEK293T cells transfected with constructs encoding HA-tagged mouse ARRB2 and Myc-tagged mouse DRD1 and DRD5 or their corresponding arrestin binding mutants (mD1Am and mD5Am).
(D) *In vitro* glutathione S-transferase (GST) pull-down assay. Lysates of BMDMs stimulated with Pam3 were incubated with GST alone or GST fused to mD1CT (mouse DRD1 CT), mD5CT (mouse DRD5 CT), and mD5CTEFDm (mouse DRD5 CT EFD motif mutant), followed by incubation with glutathione Magbeads to pull down binding proteins, and analyzed by immunoblotting with TRAF6 antibody.
(E) BMDMs were treated as indicated for 1 h. Cell lysates were immunoprecipitated with anti-DRD5 antibody. Immunoprecipitates and cell lysates (input) were probed for ARRB2, PP2Ac, TRAF6, TAK1, IKKβ, p38, and DRD5 by immunoblotting.
Data are representative of three experiments.
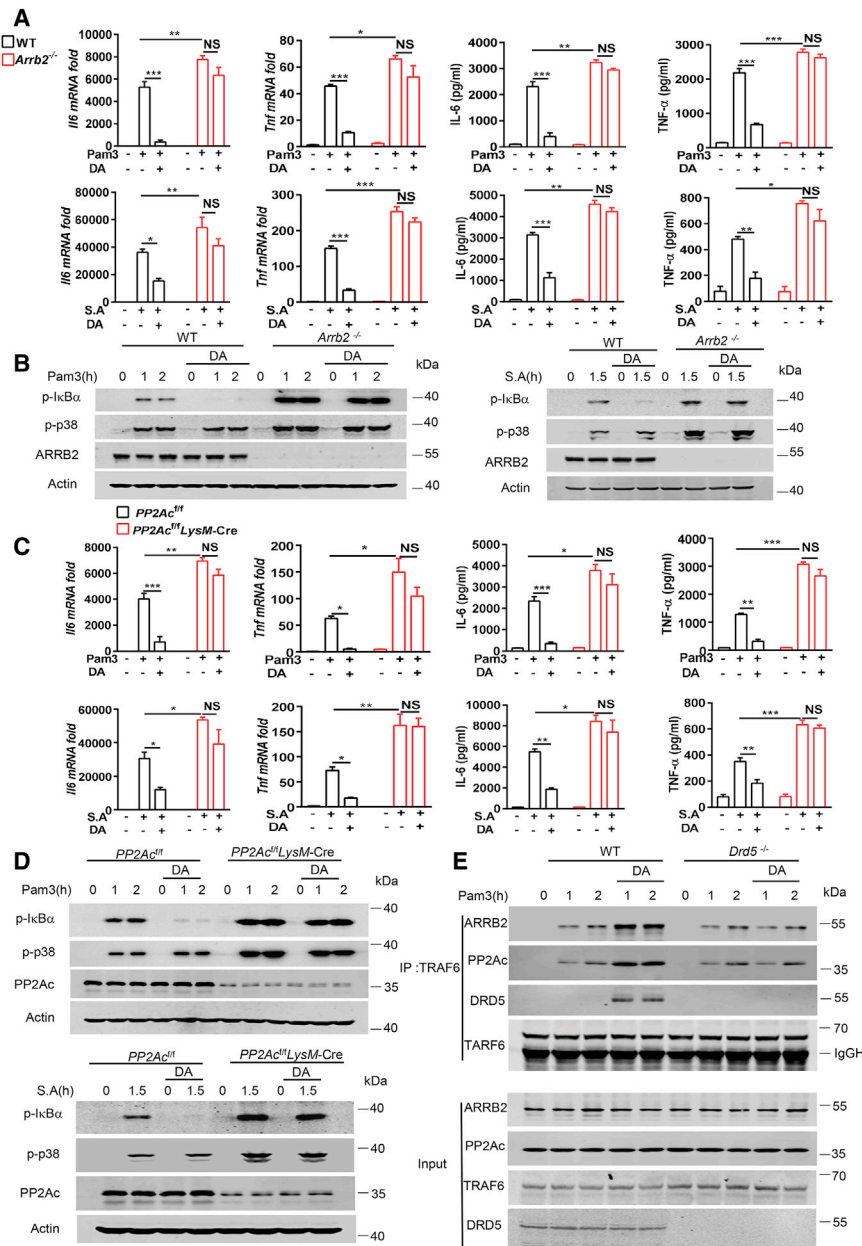See also Figure 4 and Figure S7.

Figure 6. Inhibition of TLR2-Induced Inflammation by DRD5 Activation Requires the ARRB2/PP2A Signaling Complex

(A) Left: qRT-PCR analysis of *Il6* and *Tnf* mRNA expression in WT and *Arrb2*$^{−/−}$ BMDMs treated as indicated for 6 h. ELISA of IL-6 and TNF-α in supernatants from WT and *Arrb2*$^{−/−}$ BMDMs treated as indicated for 18 h.

(B) Immunoblot analysis of p-IκBα, p-p38, and ARRB2 in lysates of WT and *Arrb2*$^{−/−}$ BMDMs treated as indicated.

(C) Left: qRT-PCR analysis of *Il6* and *Tnf* mRNA expression in *PP2Ac*$^{f/f}$ and *PP2Ac*$^{f/f}$*LysM*-Cre BMDMs treated as indicated for 6 h. Right: ELISA of IL-6 and TNF-α in supernatants from *PP2Ac*$^{f/f}$ and *PP2Ac*$^{f/f}$*LysM*-Cre BMDMs treated as indicated for 18 h.

(D) Immunoblot analysis of p-IκBα, p-p38, and PP2Ac in lysates of *PP2Ac*$^{f/f}$ and *PP2Ac*$^{f/f}$*LysM*-Cre BMDMs treated as indicated.

(E) WT and *Drd5*$^{−/−}$ BMDMs were treated as indicated. Cell lysates were immunoprecipitated with anti-TRAF6 antibody. Immunoprecipitates and cell lysates (input) were probed for ARRB2, PP2Ac, DRD5, and TRAF6 by immunoblotting.

Data are pooled from three independent experiments (A and C) or representative of three independent experiments (B, D, and E). Error bars show means ± SEM. *p < 0.05, **p < 0.01, ***p < 0.001; NS, not significant. Two-way ANOVA with Sidak's multiple comparisons test for (A) and (C). See also Figures S4, S5, and S7.

of BMDMs induced by Pam3, an inflammasome-independent TLR inflammatory activator, and specifically found that the top downregulated pathway by DA was the NF-κB inflammatory signaling pathway. This is consistent with the recent studies of Wang et al. (2019) and Lu et al. (2019), showing that DA blocks the NF-κB pathway and inflammation, but no details are provided regarding an underlying mechanism. Primary macrophages express all DRDs on the surface (Talhada et al., 2018). However, the function of DA-DRD5 signaling in macro-

analysis, IBA1 immunostaining also revealed that SKF-38393 treatment strongly reduced the numbers of activated microglia and peripheral myeloid cells of the brain in WT mice after *S. aureus* infection but had little effect on *Drd5*$^{−/−}$, *Arrb2*$^{−/−}$, and *PP2Ac*$^{f/f}$*LysM*-Cre mice (Figure 7D). These results suggest that the DRD5-ARRB2-PP2A signaling axis can prevent *S. aureus*-induced neuroinflammation and meningitis.

DISCUSSION

The function and mechanism underlying the inhibitory effects of DA on inflammation remain to be defined. In this study, we utilized RNA-seq to analyze the changes in transcriptional profiles

phages remains unknown. Here we observed that DRD5 is a unique receptor subtype whose expression in BMDMs and human PBMCs was significantly increased after Pam3 stimulation or *S. aureus* infection. We further utilized DRD-specific agonists and knockdown and knockout cells to demonstrate that DRD5 plays a critical role, whereas DRD1, DRD2, DRD3, and DRD4 have no roles in DA-mediated inhibition of TLR2 or *S. aureus*-induced NF-κB activation and inflammation. Our results provide first insights into the function of DA-DRD5 signaling in mediating the anti-inflammatory effects of DA in macrophages.

As G protein-coupled receptor (GPCR) members, the D1-like receptors DRD1 and DRD5 initiate their biological function by coupling to G proteins, and their stimulation leads to activity of
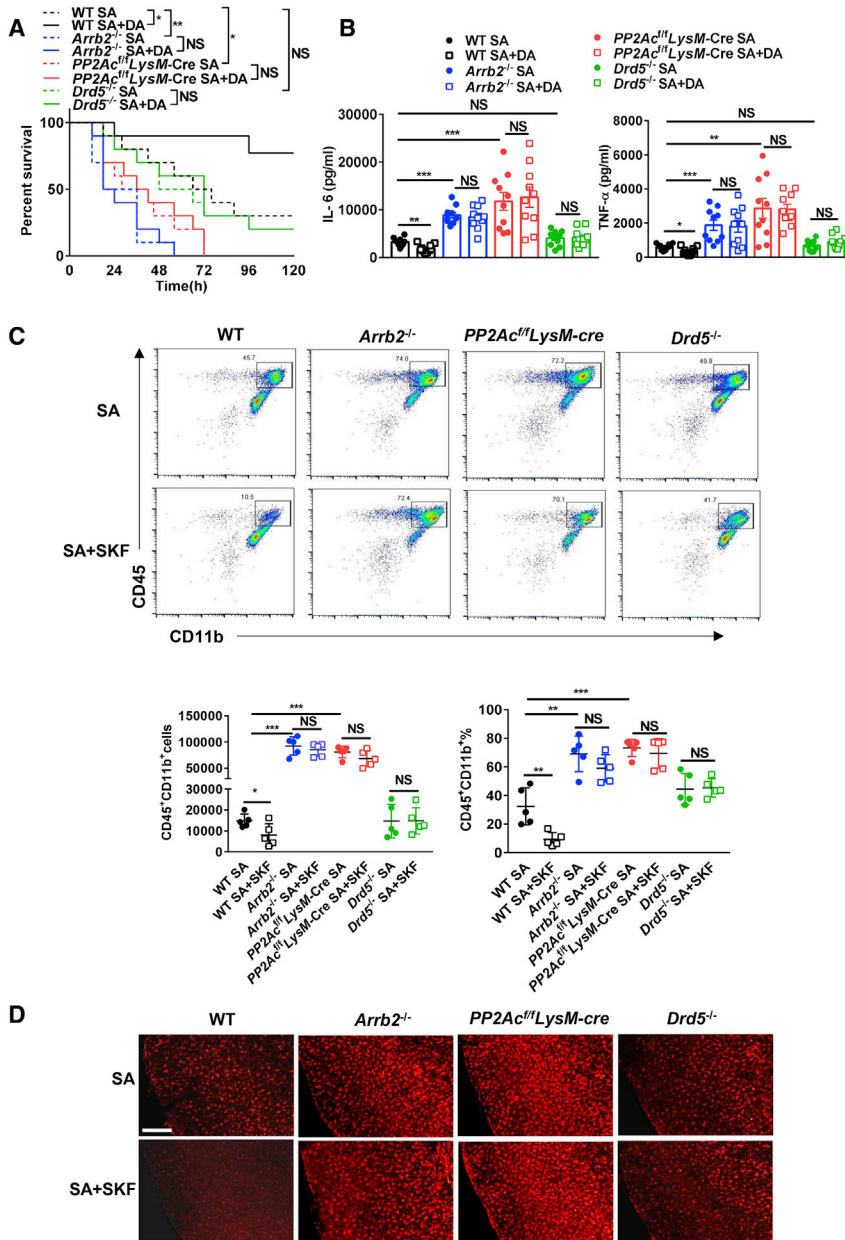
Figure 7. DRD5-ARRB2-PP2A Signaling Activation Prevents *S. aureus*-Induced Sepsis and Meningitis

(A) Survival of WT, $Drd5^{-/-}$, $Arrb2^{-/-}$, and $PP2Ac^{f/f}$ LysM-Cre mice injected intraperitoneally (i.p.) injected with *S. aureus* with or without DA (50 mg/ml of body weight).

(B) ELISA of IL-6 and TNF-α in sera of WT, $Drd5^{-/-}$, $Arrb2^{-/-}$, and $PP2Ac^{f/f}$ LysM-Cre mice 12 h after infection with *S. aureus* with or without DA administration.

(C) Flow cytometry analysis of activated microglia and peripheral myeloid cells (CD11b$^+$CD45^{high}) in brains from WT, $Drd5^{-/-}$, $Arrb2^{-/-}$, and $PP2Ac^{f/f}$ LysM-Cre mice 36 h after intravenous (i.v.) injection with *S. aureus* with or without SKF-38393 (10 mg/kg of body weight).

(D) Immunofluorescence analysis of IBA1 in cortices of WT, $Drd5^{-/-}$, $Arrb2^{-/-}$, and $PP2Ac^{f/f}$ LysM-Cre mice 36 h after i.v. injection with *S. aureus* with or without SKF-38393. Scale bars, 100 μm.

Data are pooled from three independent experiments. Error bars show means ± SEM. *p < 0.05, **p < 0.01, ***p < 0.001; NS, not significant. Log rank (Mantel-Cox) test for (A), unpaired t test for (B) and (C).

See also Figures S6 and S7.

Most GPCRs have a very large cytoplasmic IC3 loop or CT. DR elements involved in ARRB2 binding have been identified to be in the IC3 loop, and a previous study suggested that the IYIVL sequence at the N terminus of the IC3 loop of DRD2 is important for its ARRB2 binding (Lan et al., 2009). In this study, we further identified the IYRI sequence (termed the IYX(X)I/L motif in this study) at the N terminus of IC3 of DRD5 to be required for binding of ARRB2, and this sequence is highly conserved across species. Furthermore, although there is no classic P-X-E-X-X-Ar/Ac TRAF6-binding motif in DRD5, we observed a region rich in Ac and Ar amino acids, including glutamate (E), aspartate (D), and phenylalanine (F) (called the EFD motif in this study) at the CT of DRD5,

ADCY and production of cAMP, which subsequently activates downstream PKA signaling (Beaulieu and Gainetdinov, 2011). Although PKA signaling has been reported to play diverse and complex roles in the regulation of NF-κB (Gerlo et al., 2011), we did not observe any roles of cAMP or PKA in DA-mediated inhibitory effects on TLR2-induced NF-κB activity and subsequent inflammation. In contrast, we found that, upon activation by DA, DRD5 can directly recruit TRAF6, a NF-κB signaling key player, and its negative regulator ARRB2 through the EFD and IYX(X)I/L motifs in the CT and IC3 loop, respectively, of DRD5 and subsequently form a multi-protein complex containing ARRB2, TRAF6, and their downstream factors to negatively regulate TRAF6-dependent NF-κB inflammatory signaling.

which is highly conserved in different species and necessary for direct interaction between DRD5 and TRAF6. To our present knowledge, such a TRAF6-binding motif has not yet been reported. The exact structure and nature of interaction between the DRD5 CT EFD motif and TRAF6 needs to be determined by future X-ray crystal studies. Given that TRAF6 dissociates from TLRs after TLR activation to form transduction complexes with NF-κB signaling-associated proteins, such as TAK1 and IKKs (Takeda and Akira, 2004), we propose a model in which, upon TLR2 and DRD5 signaling activation, TRAF6, its negative regulator ARRB2, and their downstream proteins, including TAK1, IKKs, and PP2A, can be recruited by DRD5 to form a multi-protein complex, facilitating negative regulation of

TRAF6-dependent NF-κB inflammatory signaling by ARRB2/PP2A (Figure S7).

DRD1 signaling has been found to negatively regulate the NLRP3 inflammasome via cAMP, which binds to NLRP3 and promotes its ubiquitination and degradation by the E3 ubiquitin ligase MARCH7, blocking maturation and secretion of IL-1β and IL-18 (Yan et al., 2015). Here we found that DRD5 signaling utilizes a mechanism independent of cAMP-PKA signaling to directly recruit TRAF6 and its negative regulator ARRB2 and subsequently form a multi-protein complex containing ARRB2, TRAF6, and their downstream factors, negatively regulating TRAF6-dependent NF-κB inflammatory signaling. We speculate that D1 and D5 signaling adopt different mechanisms and integrate them to collectively target inflammation, which may be the result of long-term evolution of our immune system to fight against various G^+ or G^- bacterial infection and inflammatory responses in a variety of ways. This further highlights that DA signaling plays an important role in regulation of the immune inflammatory response.

Although endogenous DA lacks an effect on controlling inflammation in an acute infection model, we cannot exclude the possibility that endogenous DA has roles in limiting inflammation in other chronic inflammatory diseases. Altogether, our study maps an entirely new neuroimmune regulatory signaling pathway that controls systemic inflammation induced by G^+ bacteria. Development of therapeutic strategies to specifically target DA-DRD5 signaling might be useful for protection against *S. aureus* infection-induced inflammatory disease.

STAR★METHODS

Detailed methods are provided in the online version of this paper and include the following:

- KEY RESOURCES TABLE
- LEAD CONTACT AND MATERIALS AVAILABILITY
- EXPERIMENTAL MODEL AND SUBJECT DETAILS
  - Mice
- METHOD DETAILS
  - Cell culture
  - Expression vectors
  - RT-qPCR
  - ELISA
  - siRNA-Mediated Gene Silences in BMDMs
  - Functional rescue of primary DRD5-deficient BMDMs
  - Immunostaining, confocal microscopy
  - Immunoprecipitation and immunoblot analysis
  - Luciferase reporter assay
  - Generation of recombinant proteins and *in vitro* pull-down assays
  - RNA-Seq
  - Flow cytometry
  - S. aureus-induced systemic inflammation and neuroinflammation
  - HPLC analysis
  - Bacterial burden
- QUANTIFICATION AND STATISTICAL ANALYSIS
- DATA AND CODE AVAILABILITY

SUPPLEMENTAL INFORMATION

Supplemental Information can be found online at https://doi.org/10.1016/j.molcel.2020.01.022.

AUTHOR CONTRIBUTIONS

Y.W., Y.H., S.L., C.M., and X.L. designed and performed the experiments, analyzed the data, and prepared the figures. B.W. and J.Z. provided key technique mentoring, research reagents, and mice. B.W., P.N.M., and J.Z. contributed to the experimental design and edited the manuscript. S.Y. supervised the project. Y.W., Y.H., and S.Y. wrote the manuscript.

DECLARATION OF INTERESTS

The authors declare no competing interests.

REFERENCES

Beaulieu, J.M., and Gainetdinov, R.R. (2011). The physiology, signaling, and pharmacology of dopamine receptors. Pharmacol. Rev. *63*, 182–217.

Beaulieu, J.M., Sotnikova, T.D., Marion, S., Lefkowitz, R.J., Gainetdinov, R.R., and Caron, M.G. (2005). An Akt/beta-arrestin 2/PP2A signaling complex mediates dopaminergic neurotransmission and behavior. Cell *122*, 261–273.

Borovikova, L.V., Ivanova, S., Zhang, M., Yang, H., Botchkina, G.I., Watkins, L.R., Wang, H., Abumrad, N., Eaton, J.W., and Tracey, K.J. (2000). Vagus nerve stimulation attenuates the systemic inflammatory response to endotoxin. Nature *405*, 458–462.

Chen, G.Y., and Nuñez, G. (2010). Sterile inflammation: sensing and reacting to damage. Nat. Rev. Immunol. *10*, 826–837.

Daubner, S.C., Le, T., and Wang, S. (2011). Tyrosine hydroxylase and regulation of dopamine synthesis. Arch. Biochem. Biophys. *508*, 1–12.

Free, R.B., Hazelwood, L.A., Cabrera, D.M., Spalding, H.N., Namkung, Y., Rankin, M.L., and Sibley, D.R. (2007). D1 and D2 dopamine receptor expression is regulated by direct interaction with the chaperone protein calnexin. J. Biol. Chem. *282*, 21285–21300.

Gerlo, S., Kooijman, R., Beck, I.M., Kolmus, K., Spooren, A., and Haegeman, G. (2011). Cyclic AMP: a selective modulator of NF-κB action. Cell. Mol. Life Sci. *68*, 3823–3841.

Hayden, M.S., and Ghosh, S. (2012). NF-κB, the first quarter-century: remarkable progress and outstanding questions. Genes Dev. *26*, 203–234.

Jiang, X., and Chen, Z.J. (2011). The role of ubiquitylation in immune defence and pathogen evasion. Nat. Rev. Immunol. *12*, 35–48.

Kawai, T., and Akira, S. (2007). Signaling to NF-kappaB by Toll-like receptors. Trends Mol. Med. *13*, 460–469.

Kitur, K., Wachtel, S., Brown, A., Wickersham, M., Paulino, F., Peñaloza, H.F., Soong, G., Bueno, S., Parker, D., and Prince, A. (2016). Necroptosis promotes Staphylococcus aureus clearance by inhibiting excessive inflammatory signaling. Cell Rep. 16, 2219–2230.

Lan, H., Liu, Y., Bell, M.I., Gurevich, V.V., and Neve, K.A. (2009). A dopamine D2 receptor mutant capable of G protein-mediated signaling but deficient in arrestin binding. Mol. Pharmacol. 75, 113–123.

Leech, J.M., Lacey, K.A., Mulcahy, M.E., Medina, E., and McLoughlin, R.M. (2017). IL-10 plays opposing roles during Staphylococcus aureus systemic and localized infections. J. Immunol. 198, 2352–2365.

Liu, S., Cai, X., Wu, J., Cong, Q., Chen, X., Li, T., Du, F., Ren, J., Wu, Y.T., Grishin, N.V., and Chen, Z.J. (2015). Phosphorylation of innate immune adaptor proteins MAVS, STING, and TRIF induces IRF3 activation. Science 347, aaa2630.

Lu, W., Ding, Z., Liu, F., Shan, W., Cheng, C., Xu, J., He, W., Huang, W., Ma, J., and Yin, Z. (2019). Dopamine delays articular cartilage degradation in osteoarthritis by negative regulation of the NF-κB and JAK2/STAT3 signaling pathways. Biomed. Pharmacother. 119, 109419.

Luttrell, L.M., and Lefkowitz, R.J. (2002). The role of beta-arrestins in the termination and transduction of G-protein-coupled receptor signals. J. Cell Sci. 115, 455–465.

Medzhitov, R. (2008). Origin and physiological roles of inflammation. Nature 454, 428–435.

Missale, C., Nash, S.R., Robinson, S.W., Jaber, M., and Caron, M.G. (1998). Dopamine receptors: from structure to function. Physiol. Rev. 78, 189–225.

Nakai, A., Hayano, Y., Furuta, F., Noda, M., and Suzuki, K. (2014). Control of lymphocyte egress from lymph nodes through β2-adrenergic receptors. J. Exp. Med. 211, 2583–2598.

Neve, K.A., Seamans, J.K., and Trantham-Davidson, H. (2004). Dopamine receptor signaling. J. Recept. Signal Transduct. Res. 24, 165–205.

Nieoullon, A. (2002). Dopamine and the regulation of cognition and attention. Prog. Neurobiol. 67, 53–83.

Oliveira-Nascimento, L., Massari, P., and Wetzler, L.M. (2012). The Role of TLR2 in Infection and Immunity. Front. Immunol. 3, 79.

Ozinsky, A., Underhill, D.M., Fontenot, J.D., Hajjar, A.M., Smith, K.D., Wilson, C.B., Schroeder, L., and Aderem, A. (2000). The repertoire for pattern recognition of pathogens by the innate immune system is defined by cooperation between toll-like receptors. Proc. Natl. Acad. Sci. USA 97, 13766–13771.

Pacheco, R., Contreras, F., and Zouali, M. (2014). The dopaminergic system in autoimmune diseases. Front. Immunol. 5, 117.

Papa, I., Saliba, D., Ponzoni, M., Bustamante, S., Canete, P.F., Gonzalez-Figueroa, P., McNamara, H.A., Valvo, S., Grimbaldeston, M., Sweet, R.A., et al. (2017). T_FH-derived dopamine accelerates productive synapses in germinal centres. Nature 547, 318–323.

Pavlov, V.A., Chavan, S.S., and Tracey, K.J. (2018). Molecular and Functional Neuroscience in Immunity. Annu. Rev. Immunol. 36, 783–812.

Rosas-Ballina, M., and Tracey, K.J. (2009). Cholinergic control of inflammation. J. Intern. Med. 265, 663–679.

Shao, W., Zhang, S.Z., Tang, M., Zhang, X.H., Zhou, Z., Yin, Y.Q., Zhou, Q.B., Huang, Y.Y., Liu, Y.J., Wawrousek, E., et al. (2013). Suppression of neuroinflammation by astrocytic dopamine D2 receptors via αB-crystallin. Nature 494, 90–94.

Takeda, K., and Akira, S. (2004). TLR signaling pathways. Semin. Immunol. 16, 3–9.

Takeuchi, O., and Akira, S. (2010). Pattern recognition receptors and inflammation. Cell 140, 805–820.

Talhada, D., Rabenstein, M., and Ruscher, K. (2018). The role of dopaminergic immune cell signalling in poststroke inflammation. Ther. Adv. Neurol. Disorder. 11, 1756286418774225.

Tong, S.Y., Davis, J.S., Eichenberger, E., Holland, T.L., and Fowler, V.G., Jr. (2015). Staphylococcus aureus infections: epidemiology, pathophysiology, clinical manifestations, and management. Clin. Microbiol. Rev. 28, 603–661.

Torres-Rosas, R., Yehia, G., Peña, G., Mishra, P., del Rocio Thompson-Bonilla, M., Moreno-Eutimio, M.A., Arriaga-Pizano, L.A., Isibasi, A., and Ulloa, L. (2014). Dopamine mediates vagal modulation of the immune system by electroacupuncture. Nat. Med. 20, 291–295.

Wang, Y., Tang, Y., Teng, L., Wu, Y., Zhao, X., and Pei, G. (2006). Association of beta-arrestin and TRAF6 negatively regulates Toll-like receptor-interleukin 1 receptor signaling. Nat. Immunol. 7, 139–147.

Wang, B., Chen, T., Li, G., Jia, Y., Wang, J., Xue, L., and Chen, Y. (2019). Dopamine alters lipopolysaccharide-induced nitric oxide production in microglial cells via activation of D1-like receptors. Neurochem. Res. 44, 947–958.

Witt, J., Barisic, S., Schumann, E., Allgöwer, F., Sawodny, O., Sauter, T., and Kulms, D. (2009). Mechanism of PP2A-mediated IKK beta dephosphorylation: a systems biological approach. BMC Syst. Biol. 3, 71.

Yamamoto, M., Sato, S., Hemmi, H., Hoshino, K., Kaisho, T., Sanjo, H., Takeuchi, O., Sugiyama, M., Okabe, M., Takeda, K., and Akira, S. (2003). Role of adaptor TRIF in the MyD88-independent toll-like receptor signaling pathway. Science 301, 640–643.

Yan, Y., Jiang, W., Liu, L., Wang, X., Ding, C., Tian, Z., and Zhou, R. (2015). Dopamine controls systemic inflammation through inhibition of NLRP3 inflammasome. Cell 160, 62–73.

Ye, H., Arron, J.R., Lamothe, B., Cirilli, M., Kobayashi, T., Shevde, N.K., Segal, D., Dzivenu, O.K., Vologodskaia, M., Yim, M., et al. (2002). Distinct molecular mechanism for initiating TRAF6 signalling. Nature 418, 443–447.

Youdim, M.B., Edmondson, D., and Tipton, K.F. (2006). The therapeutic potential of monoamine oxidase inhibitors. Nat. Rev. Neurosci. 7, 295–309.

STAR★METHODS

KEY RESOURCES TABLE

REAGENT or RESOURCE	SOURCE	IDENTIFIER
Antibodies		
p-IκBα	Cell Signaling Technology	Cat#9246; RRID: AB_2267145
p-JNK	Cell Signaling Technology	Cat#9251; RRID: AB_331659
p-p38	Cell Signaling Technology	Cat#9211; RRID: AB_331641
p-IKKα/β	Cell Signaling Technology	Cat#2697; RRID: AB_2079382
JNK	Cell Signaling Technology	Cat#9252; RRID: AB_2250373
p38	Cell Signaling Technology	Cat#9212; RRID: AB_330713
IKKβ	Cell Signaling Technology	Cat#2370; RRID: AB_2122154
MYC	Cell Signaling Technology	Cat#2276; RRID: AB_331783
FLAG	Sigma-Aldrich	Cat#F3165; RRID: AB_259529
actin	Sigma-Aldrich	Cat#A1978; RRID: AB_476692
HA	Covance	Cat#16B12; RRID: AB_10063630
TRAF6	Santa Cruz	Cat#sc-7221; RRID: AB_793346
IBA1	abcam	Cat#019-19741; RRID: AB_839504
DRD1	Hangzhou HuaAn Biotechnology	Cat#ET1703-45; RRID: AB_ 2815007
DRD2	Bioss	Cat#bs-20730R; RRID: AB_ 2815008
DRD3	Affinity	Cat#DF10212; RRID: AB_ 2815010
DRD4	Bioss	Cat#bs-1746R; RRID: AB_ 10857578
DRD5	Santa Cruz	Cat#sc-33661; RRID: AB_673639
DRD5	Proteintech	Cat#20310-1-AP; RRID: AB_10699880
β-arrestin2	Santa Cruz	Cat#sc-13140; RRID: AB_626701
β-arrestin2	Proteintech	Cat#10171-1-AP; RRID: AB_10644158
IRDye 680RD-anti-mouse	LI-COR Biosciences	Cat#926-68070; RRID: AB_10956588
IRDye 800CW-anti-rabbit	LI-COR Biosciences	Cat#926-32211; RRID: AB_621843
Anti-mouse-HRP	Invitrogen	Cat#31430; RRID: AB_228307
Anti-rabbit-HRP	Invitrogen	Cat#31460; RRID: AB_228341
CD45-AF700	eBioscience	Cat#56-0451-80; RRID: AB_891456
CD11b- FITC	eBioscience	Cat#11-0112-82; RRID: AB_464935
Bacterial and Virus Strains		
Staphylococcus aureus	ATCC	Cat#25923
Chemicals, Peptides, and Recombinant Proteins		
LPS	EnzoLife Sciences	Cat#ALX-581013L002
Pam3CSK4	Invivogen	Cat#Tlrl-pms
Poly(I:C)	Invivogen	Cat#PLC-37-07
RecFLA-ST	Invivogen	Cat#Tlrl-flic-10
CL097	Invivogen	Cat#Tlrl-C97
ODN2395	Invivogen	Cat#Tlrl-2395
SKF-38393 hydrobromide	TOCRIS	Cat#0922
Phenelzine sulfate salt	Sigma-Aldrich	Cat#P6777
3,5-Dinitrocatechol	Sigma-Aldrich	Cat#D131
A-68930 hydrochloride	Sigma-Aldrich	Cat#1534
Quinpirole	Sigma-Aldrich	Cat#096K4603
H89	CSNpharm	Cat#CSN11132
KH7	MedChemExpress	Cat#103194

(Continued on next page)

Continued

REAGENT or RESOURCE	SOURCE	IDENTIFIER
Trizol	Life technologies	Cat#15596018
Dopamine hydrochloride	Sigma-Aldrich	Cat#H8502
AceQ qPCR SYBR Green Master Mix	Vazyme	Cat#Q111-02
4',6-Diamidino-2-phenylindoledihydrochloride (DAPI)	Sigma-Aldrich	Cat#D9542
Anti-Myc magnetic beads	Biomake	Cat#B26301
Critical Commercial Assays		
Mouse IL-6 DuoSet ELISA	R&D Systems	Cat#DY406
Mouse TNF-alpha DuoSet ELISA	R&D Systems	Cat#DY410
Mouse IL-12/IL-23 p40 Non Allele-specific DuoSet	R&D Systems	Cat#DY2398
Deposited Data		
RNA-seq	NCBI Gene Expression Omnibus	GSE 133316
Raw images of western blots and original image files	Mendeley Data	https://doi.org/10.17632/r68gw2wbwy.1
Experimental Models: Cell Lines		
Human:HEK293T	ATCC	Cat#CRL-11268
Mouse:Primary bone marrow-derived macrophages	This paper	N/A
Experimental Models: Organisms/Strains		
Mouse: C57BL/6J	The Jackson Laboratory	Stock No: 000664
Mouse: $Drd1^{-/-}$	Dr. Jiawei Zhou, SIBS,China	N/A
Mouse: $Drd2^{-/-}$	Dr. Jiawei Zhou, SIBS,China	N/A
Mouse:$Arrb2^{-/-}$	Dr. Gang Pei, Tongji University,China	N/A
Mouse:$PP2Ac^{fl/fl}$	Dr. Xiang Gao, Nanjing University,China & Dr. Jun Gao, Nanjing Medical University,China	N/A
Mouse:$LysM$-Cre	The Jackson Laboratory	Stock No:004781
Mouse:$Drd5^{-/-}$	Cyagen Biosciences Inc	N/A
Oligonucleotides		
See Table S1 for oligonucleotide information	This paper	N/A
Recombinant DNA		
Plasmid: human DRD1	Dr. Jiawei Zhou, SIBS,China	N/A
Plasmid: human DRD2	Dr. Jiawei Zhou, SIBS,China	N/A
Plasmid: human DRD3	Addgene	Cat#24098
Plasmid: human DRD4	Addgene	Cat#24100
Plasmid: human DRD5	Addgene	Cat#66272
Plasmid: mouse DRD1	OriGene	Cat# MR226226
Plasmid: mouse DRD3	OriGene	Cat# MR226047
Plasmid: mouse DRD5	OriGene	Cat# MR222905
Plasmid: mouse ARRB2	OriGene	Cat# MR206444
Plasmid: mouse PP2Ac	Dr. Dong Xie,SIBS, China	N/A
Plasmid: human ARRB2	Dr. Gang Pei, Tongji University,China	N/A
Plasmid: pLV-mD5	This paper	N/A
Plasmid: pLV-mD5Am	This paper	N/A
Plasmid: pLV-mD5EFDm	This paper	N/A
Plasmid: pcDNA3.1- hD1Am	This paper	N/A
Plasmid: pcDNA3.1- hD3Am	This paper	N/A
Plasmid: pcDNA3.1- hD5Am	This paper	N/A
Plasmid: pcDNA3.1- mD1Am	This paper	N/A
Plasmid: pcDNA3.1- mD5Am	This paper	N/A
Plasmid: pcDNA3.1- hD1IC3 dm	This paper	N/A

Continued

REAGENT or RESOURCE	SOURCE	IDENTIFIER
Plasmid: pcDNA3.1- hD1CTdm	This paper	N/A
Plasmid: pcDNA3.1- hD3IC3 dm	This paper	N/A
Plasmid: pcDNA3.1- hD5CTdm	This paper	N/A
Plasmid: pcDNA3.1- mD5CTdm	This paper	N/A
Plasmid: pcDNA3.1- hD5EFDm	This paper	N/A
Plasmid: pcDNA3.1- mD5EFDm	This paper	N/A
Plasmid: pGEX6P1-GST-mD1CT	This paper	N/A
Plasmid: pGEX6P1- GST-mD5CT	This paper	N/A
Plasmid: pGEX6P1- GST-mD5CTEFDm	This paper	N/A
Software and Algorithms		
FlowJo Software (version 10.5.3)	FlowJo	https://www.flowjo.com/
GraphPad Prism 7	GraphPad Software	https://www.graphpad.com
ImageJ 1.49V	ImageJ	https://imagej.nih.gov

LEAD CONTACT AND MATERIALS AVAILABILITY

Further information and requests for resources and reagents should be directed to and will be fulfilled by the Lead Contact, Shuo Yang (shuoyang@njmu.edu.cn).

EXPERIMENTAL MODEL AND SUBJECT DETAILS

Mice

The $Drd1^{-/-}$ and $Drd2^{-/-}$ (The Jackson Laboratory) mice were provided by Dr. Jiawei Zhou. The $Arrb2^{-/-}$ mice were provided by Dr. Gang Pei (Tongji University). $PP2Ac^{fl/fl}$ mice were provided by Dr. Xiang Gao (Nanjing University) and Dr. Jun Gao (Nanjing Medical University). $PP2Ac$ floxed mice were crossed with lysozyme cre mice (*LysM*-Cre; The Jackson Laboratory) to generate myeloid cell-conditional PP2Ac knockout mice ($PP2Ac^{fl/fl}$ *LysM*-Cre). $Drd5^{-/-}$ mice were generated by Cyagen Biosciences Inc (Guangzhou, China) using CRISPR-Cas9 technology, performed by co-microinjection of *in vitro*-translated Cas9 mRNA and gRNA into the C57BL/6 zygotes. The two gRNA sequences used were CCCGCGAGCACCGGTCGCTTCC and CTCATGGGCATGTACAGTTGTG. Two lines of $Drd5^{-/-}$ mice were generated that modified the $Drd5$ gene in different ways. One contained a 1725 bp deletion and 9 bp insertion, and the other contained a 1725 bp deletion. F0 founders were bred to wild-type mice to test germline transmission and F1 animal generation. After genotyping for confirmation, the founders were intercrossed to generate biallelic Drd5 deficiency mice, which were identified again followed by sequence analysis. Mice were genotyped by PCR analysis of DNA isolated from ear punches using forward primers F1(5′-GGCCTCTGCGATCCACTTCTTC-3′), reverse primers R1(5′-GAAAGTCACAGACCATACCAGC-3′) and reverse primers R2(5′-CTTTAATGGTATCAGTCTTGCGCG-3′); The 439 bp fragment for the wild-type allele and the 670 bp fragment for Drd5 heterozygous allele were reconfirmed. All mice were kept in a barrier facility, and all animal experiments were conducted in accordance with the procedure approved by the Ethical Review Committee for Laboratory Animal Welfare of Nanjing Medical University.

METHOD DETAILS

Cell culture

HEK293T cells were cultured in Dulbecco's modified Eagle's medium supplemented with 10% (v/v) fetal bovine serum (FBS),100 ug/ml penicillin G and 100 ug/ml streptomycin. For isolation of BMDMs, tibias and femurs were removed from wild-type and knockout mice by sterile techniques and the bone marrow was flushed with fresh medium. BMDMs were plated in DMEM supplemented with 10% FBS in the presence of 10% L929 conditioned medium for 4–6 d at 37°C in a humidified atmosphere of 5% CO_2.

Expression vectors

DRD1, DRD2 of human origin were from Dr. Jiawei Zhou. DRD3 (24098), DRD4 (24100) and DRD5 (66272) of human origin were obtained from Addgene. DRD1 (MR226226), DRD3 (MR226047) and DRD5 (MR222905) of mouse origin were purchased from OriGene. All of human and mouse DRD receptors were cloned into pcDNA3.1 vector with Myc tag at the carboxy terminus. The IYX(X)I/L motif of hDRD1, hDRD3, hDRD5, mDRD1, mDRD5 were mutated to alanine for generating the substitution mutants: hD1Am, hD3Am,

hD5Am, mD1Am, mD5Am. The third intracellular loop (IC3) and cytoplasmic C-terminal tail (CT) deletion mutants of DRD1, DRD3 and DRD5 (including hD1IC3 dm, hD1CTdm, hD3IC3 dm, hD5CTdm, mD5CTdm) and EFD motif mutants of DRD5 (including hD5EFDm and mD5EFDm) were generated in-house. Myc-tagged PP2Ac was gift from Dr. Dong Xie (SIBS) and HA-tagged ARRB2 of human origin was gift from Dr. Gang Pei (Tongji University). ARRB2 (MR206444) of mouse origin was purchased from OriGene and cloned into pcDNA3.1 vector with HA tag at the carboxy terminus.

For rescue experiment, wild-type and mutants of mouse DRD5 (including pLV-mD5, pLV-mD5Am and pLV-mD5EFDm) were cloned into the lentiviral vectors pLV-EF1a-IRES-GFP (Addgene) with Flag tag at the carboxy terminus. For recombinant protein expression, Flag-tagged wide type and EFD motif mutant of cytoplasmic C-terminal tail (CT) of DRDs (including GST-mD1CT, GST-mD5CT and GST-mD5CTEFDm) were cloned into pGEX6P1 Vector. All plasmids were verified by DNA sequencing.

RT-qPCR
Total RNA was extracted by using TRIzol reagent (Life) and subjected to cDNA synthesis. qRT-PCR was performed using AceQ qPCR SYBR Green Master Mix (Vazyme). The expression of a single gene was calculated by a standard curve method and standardized to the expression of *Hprt*.

ELISA
Primary BMDMs were seeded (1.5×10^6 cells per well) in 12-well plates and were grown for 24 h. Cells were then stimulated as indicated in figure legends. Conditioned media were collected and measured for levels of IL-6 (DY406), TNF-α (DY410) and IL-12 (DY2398) according to manufacturer's instructions (R&D Systems). The serum from wide type and genetically deficient mice were collected after infection as indicated and the levels of IL-6(DY406) and TNF-α(DY410) in these samples were measured by sandwich ELISA (R&D Systems).

siRNA-Mediated Gene Silences in BMDMs
BMDMs were plated in 12-well plates (1.5×10^6 cells per well) and then were transfected with 50nM siRNA using Lipofectamine RNAiMAX (Invitrogen) according to the manufacturer's guidelines. The siRNA sequences were: siDrd1 (GGGAGACUAAAGUCCU GAAdTdT), siDrd2 (GGCCAUGCCUAUGUUGUAUdTdT), siDrd3 (GGUGGAGUCUCGGGAAUUUCAdTdT), siDrd4 (CCUGGAGAACC GAGACUAUdTdT), siDrd5 (CUGCCUAUGUCCACAUGAUdTdT), siRNA was chemically synthesized by GenePharma. The negative control siRNA was from GenePharma.

Functional rescue of primary DRD5-deficient BMDMs
For rescue experiment, wild-type and mutants of mouse DRD5 (including pLV-mD5, pLV-mD5Am and pLV-mD5EFDm) were cloned into the lentiviral vectors pLV-EF1a-IRES-GFP (Addgene) with Flag tag at the carboxy termini. Constructs were transfected into HEK293T cells together with packaging and envelope plasmids (psPAX2 and pMD2.G). Plv lentivirus from the medium supernatants were collected at 48 h,72 h and 96 h. The virus was infected with wild-type and DRD5-deficient bone marrows differentiated on the second, third and fourth days respectively. After another two days, BMDMs were seeded and performed as described.

Immunostaining, confocal microscopy
BMDMs were seeded on slides overnight and then were stimulated as indicated. The cells were washed three times in chilled PBS (500 μl), fixed with 4% (v/v) paraformaldehyde (500 μl) for 20 min, permeabilized with 0.2% Triton X-100 for 10min and blocked with 10% goat serum (Vector Laboratories) for 2 h. Cells were incubated overnight at 4°C with primary antibody as indicated, and then washed and incubated with secondary antibody. Nuclei were stained with DAPI (1.5 μg/ml; Sigma) for 2 min. Cells were mounted and confocal images were captured using the × 63 objective lens (× 630 total magnification) on the Zeiss LSM800 META laser scanning confocal microscope and processed using Zeiss LSM image browser.

Immunoprecipitation and immunoblot analysis
Primary BMDMs (2×10^6 cells per ml; 10ml) were grown in 10-cm dishes and HEK293T cells (3×10^5 cells per ml;3ml) grown in six-well plates were transfected with the appropriate expression constructs. Cells were then collected in 500 μl lysis buffer (20 mM Tris-HCl, pH 7.4, containing 150 mM NaCl, 0.5% (vol/vol) Igepal, 50 mM NaF, 1 mM Na3VO4, 1 mM dithiothreitol, 1 mM phenylmethylsulfonyl fluoride and complete protease-inhibitor 'cocktail'), followed by incubation for 40 min at 4°C. Cell lysates were initially precleared by centrifugation at 14000 rpm and then followed by incubation for 24 h at 4°C with the appropriate antibody. An aliquot (40 μl) of protein A/G-agarose was added to each sample, followed by incubation overnight at 4°C. Immunoprecipitates were collected by centrifugation for 1 min with 1,000 g at 4°C and the beads were then washed four times with 500 μl lysis buffer (without Na3VO4, dithiothreitol, phenylmethylsulfonyl fluoride or protease-inhibitor 'cocktail'). An aliquot (50 μl) of SDS-PAGE sample buffer (62.5 mM Tris-HCl, pH 6.8, 10% (wt/vol) glycerol, 2% (wt/vol) SDS, 0.7 M β-mercaptoethanol and 0.001% (wt/vol) bromophenol blue) was added to the beads. Samples were resolved by SDS-PAGE, transferred to nitrocellulose membranes and analyzed by immunoblot with the appropriate antibodies.

Luciferase reporter assay

HEK293T cells (1.2×10^5 cells per ml; 200 μl) were seeded in 96-well plates. Cells were cotransfected with plasmids encoding NF-κB-regulated firefly luciferase and thymidine kinase-controlled renilla luciferase (Promega Biosciences) and expression constructs encoding ARRB2, PP2Ac and various forms of dopamine receptors. Cells were grown for another 24 h. Cell extracts were collected in Reporter Lysis Buffer (Promega Biosciences), and firefly and renilla luciferase activity was assayed with the Luciferase Assay system (Promega Biosciences) and coelenterazine (1 μg/ml, Insight Biotechnology), respectively.

Generation of recombinant proteins and *in vitro* pull-down assays

The C-terminal tail of mouse DRD1 and DRD5, and EFD motif mutant of DRD5 C-terminal tail were cloned into the GST-tagged pGEX6P1 vector. The constructs were transformed into BL21 cells and Protein expression was induced overnight at 18°C with 0.4 mM isopropyl-B-D-thiogalactopyranoside (IPTG) after $OD_{600\ nm}$ reached 0.8. Cells were harvested and resuspended in a lysis buffer containing 20 mM Tris-HCl (pH 8.0), 150 mM NaCl, 0.5% (vol/vol) Igepal, 1 mM phenylmethylsulfonyl fluoride and then were sonicated. After centrifugation, the recombinant proteins were purified with Glutathione Magbeads from GenScript. Then the cell lysates dialysis through Chromatography bag (Biosharp), the purity and integrity of recombinant proteins were confirmed by SDS-PAGE followed by Coomassie staining. For pull-down assay, BMDMs treated as indicated were collected in lysis buffer (20 mM Tris-HCl, pH 7.4, containing 150 mM NaCl, 0.5% (vol/vol) Igepal, 50 mM NaF, 1 mM Na3VO4, 1 mM dithiothreitol, 1 mM phenylmethylsulfonyl fluoride and complete protease-inhibitor 'cocktail') .Then the cell lysates was incubated with the recombinant GST or GST fusion protein overnight at 4°C. An aliquot (60 μl) of Glutathione Magbeads was added to each sample, followed by incubation for 2 hours at 4°C. Then the beads were washed and an aliquot (50 μl) of SDS-PAGE sample buffer (62.5 mM Tris-HCl, pH 6.8, 10% (wt/vol) glycerol, 2% (wt/vol) SDS, 0.7 M β-mercaptoethanol and 0.001% (wt/vol) bromophenol blue) was added to the beads. Samples were resolved by SDS-PAGE followed by immunoblot with the appropriate antibodies and Coomassie staining.

RNA-Seq

RNA isolation, library construction, and sequencing were performed on a BGISEQ-500 (Beijing Genomic Institution, BGI). Clean reads were mapped to the mouse genome (GRCm38.p5) by HISAT2. For gene expression analysis, the matched reads were calculated and then normalized to FPKM. Fold changes were calculated for all possible comparisons and a 2-fold cutoff was used to select genes with expression changes. KEGG pathway analysis was performed using the R package, using significantly differentially expressed genes (FDR $\leq$ 0.001) as target genes. Raw data files and processed files have been uploaded to Gene Expression Omnibus public database (GSE 133316).

Flow cytometry

For preparation of immune cells in the CNS, brains from Staphylococcus aureus infected mice were excised and digested at 37°C with collagenase type IV (0.5mg/ml; Sigma) and DNase I (10 U/ml; Roche) in RPMI 1640 under agitation (200 rpm) conditions for 60 min. The digested tissues were filtered through a 100 μm filter and the plunger end of syringe was used to push the cells over the filter. Homogeneous cell suspensions were centrifuged over the Percoll density gradient (GE Healthcare) and separated by collecting the interface fractions between 37% and 70% Percoll (GE Healthcare). Mononuclear cells were isolated from the interface. The cells were suspended in PBS containing 2% (w/v) FBS. After intensive washing, cells were stained with fluorochrome-conjugated surface marker antibodies for FACS analysis. The CD45 and CD11b antibodies were used.

S. aureus-induced systemic inflammation and neuroinflammation

For S. aureus-induced systemic inflammation, 8-week old male mice were administered with dopamine (50 mg/kg) by intraperitoneal (i.p.) injections twice in one day. After 6 hours following the second DA injection, mice were infected with Staphylococcus aureus (ATCC 25923, 1×10^8CFU per mouse) by i.p., and monitored eight times daily for a total of 6 days. Serum were collected from the retro-orbital plexus for ELISA analysis 6 hours after S. aureus infection. For S. aureus-induced neuroinflammation, 8-week old male mice were intravenously (i.v.) injected with 10mg/kg SKF-38393 or vehicle (saline) at 6 hours before S. aureus (5×10^8 CFU per mouse) i.v. infection. After 36 hours, brains were collected for FACS or immunofluorescence analysis.

HPLC analysis

HPLC analysis was employed to measure dopamine from whole blood, spleen and draining lymph nodes. This analysis used a DIONEX HPLC system with a Coulochem III Electrochemical Detector together with a Uniget C-18 reverse phase microbore column as the stationary phase. The mobile phase consisted of buffer [1.7 M OSA, 0.05 mM Na-EDTA, 90 mM NaH2PO4·2H2O and 50 nM C6H8O7·H2O] and acetonitrile. The flow rate was 0.2 ml/min and the working electrode was set at 350 mV versus Ag/Ag/Cl reference electrode. Detection gain was 100 nA and filter was 5 s.10 μL of the sample supernatant was directly injected into the HPLC for analysis. Standard dopamine (sigma) was used to quantify and identify the peaks on the chromatographs. The detection limits for dopamine was determined by analyzing the known concentrations of dopamine in the HPLC system under the set condition. For this purpose, standard solutions of 1 mg per ml was made with pure dopamine and diluted accordingly to the desired concentrations of the stock solutions for running on HPLC. Concentration of dopamine was determined using the following formula: $y = 17.983x + 37.011$ ($r2 = 0.999$) (y, peak area; x, analyte concentration in μM). All values of tissues were converted to final

molar concentrations by dividing original tissue weights, and multiplying the density of tissues which we averaged to be around 1 kg/L.

Bacterial burden
8-week-old C57BL/6 mice were administered 50 mg/kg of Dopamine by intraperitoneal (i.p.) injections twice in one day. After 6 hours of the second DA injection, mice were infected with SA (1×10^8 CFU per mouse) by i.p and then anesthetized to be sacrificed at 36h postinfection. Liver, spleen and draining lymph nodes were harvested and weighed, followed by homogenization with PBS. Homogenates were serially diluted in PBS and plated to determine bacterial numbers by the colony-formation assay.

QUANTIFICATION AND STATISTICAL ANALYSIS

Data are presented as the mean ± standard error of the mean (SEM). Samples were analyzed using unpaired t test for two groups and ANOVA for multiple groups. Log-rank (Mantel-Cox) test for Survival curves. In all cases, a P value of less than 0.05 was considered statistically significant.

DATA AND CODE AVAILABILITY

Original data for all figures in the paper is available at Mendeley Data (https://doi.org/10.17632/r68gw2wbwy.1).